

DESS Modélisation & Simulation en Mécanique
Département Mécanique
Université Joseph Fourier
Grenoble
France



Mechanical, Aerospace and
Manufacturing Engineering dep^t
University of Manchester Institute of
Science and Technology
United Kingdom



CFD actuator disk solutions
for a helicopter rotor in
hover flight

*« Solutions MFN d'un système de disque
pour rotor d'hélicoptère en vol stationnaire »*

Supervisor: Antonio Filippone

Chef de formation: Jean Pierre Chollet
Tuteur de stage: Jolanta Lewandowska

Sept 2003

“Users should approach all software with prudent caution and healthy skepticism, for the history of science and engineering, including the still-young history of software engineering, is littered with failed promises.”

Henry Petroski, “Failed Promises”
***American Scientist*, Vol. 82, Jan-Feb. 1994, pp.6-9.**

Contents

Preface
Symbols and notations
Abstract - Résumé

A

First Approach

Comparison of a CFD model – Semi-analytical Method

- 1 - Fundamentals of rotor aerodynamics: Momentum theory
 - Conservation laws of fluid mechanics
 - Application to hovering rotor
 - Rotor Power
 - Pressure variation
- 2 - Exact actuator disk solutions for non-uniform heavy loading and slipstream contraction developed by J.T.Conway.
 - General problem
 - Propellers with slipstream rotation
- 3 - Data provided by Conway (1998)
- 4 - First CFD approach of the problem
- 5 - CFD simulation of the problem
 - First grid
 - Second grid

B

Second Approach

“Blade Element Momentum (BEM)” and “CFD” coupled Calculations for helicopter in Hover flight

- 1 - Theoretical work
 - 1.1. Actuator disc model
 - 1.2. Blade Element Theory
- 2 - Programme generation
 - 2.1. Algorithm
 - 2.2. Subroutine
 - 2.3. Structure of the programme
- 3 - Results and discussion
- 4 - Data implementation in FLUENT
 - 4.1. Implementation
 - 4.2. Geometry and Meshes
 - 4.3. Numerical Procedure
 - 4.4. Results and discussion
 - Validation with the total pressure and thrust
 - Streamlines functions
 - Dynamic Pressure on the disc
 - Velocity profiles
 - Velocity on the z-axis

Conclusion
Appendices
References

Preface

This research work was carried out at the Department of Manufacturing and Aerospace Mechanical Engineering department of UMIST (University of Manchester Science and Technology) under the supervision of Dr Antonio Filippone.

My thanks go to my supervisor Dr Antonio Filippone for his guidance, encouragement and valuable comments throughout the process of this work. Moreover, he has given me the chance to work in his research group, what is and will be a great experience for my whole life.

Many grateful thanks to the “Fluent Guru” Vassilis Karanikolis for his assistance and his kindness.

A warm thank you to colleagues of the Department for their kindness and for their consideration: Charles Moulinec (UMIST Post-doctor), Guilhem Laurans (“Centrale Nantes” student), Romain Prunier (“INPG h.m.g.” student), David Tung (“ENSEM” student), Reza Issa (UMIST Thesis student), Jason Bassi (UMIST Thesis student), Ran Xenon (UMIST MPhil student), Toshi Fujii (UMIST MSc student) and the others...

Merci à mes parents pour m’avoir soutenu dans toutes mes démarches, que ce soit pour ce stage mais également pour l’ensemble de mes études depuis l’école primaire.

Enfin, je remercie celle qui m’a accompagné dans cette aventure aussi bien humaine que professionnelle, pour son soutien de chaque instant, pour sa patience à mon égard, et pour sa foi en mes folies.

Symbols and notations

a	Axial induction
a'	Tangential induction
A	Rotor area
C	Chord length
C_L	Lift coefficient
C_D	Drag coefficient
C_p	Pressure coefficient
C_t	Tangential force coefficient
C_n	Axial force coefficient
D	Drag force
F_t	Tangential force pr. meter
F_n	Axial force pr. meter
k	Turbulent kinetic energy
L	Lift force
\dot{m}	Mass flow rate
N	Number of blades
p	Static pressure
P	Total pressure
P_n	Pressure in tangential direction
P_t	Pressure in axial direction
r	Local radius
R	Rotor radius
Re	Reynolds number
T	Thrust force
V_0	Wind speed
V_{rel}	Relative speed
V_r	Velocity component in Radial direction
V_t	Velocity component in Tangential direction
V_z	Velocity component in Axial direction
α	Angle of attack
ε	Turbulent dissipation
ϕ	Angle of the relative velocity
ν	Laminar viscosity
ν_t	Eddy viscosity
ω	Angular velocity
ρ	Density
σ	Solidity of rotor
∞	Conditions at infinity

Abstract

The aim of this paper is to develop a CFD model in order to simplify the modeling of the flow induced by a helicopter rotor in hover flight. The main rotor blades are considered as a whole disc where diverse velocities and pressures are applied. If this simplification provides good results, the modeler will obtain high-quality approximations of the aerodynamic flow induced by the helicopter blades, whatever its number and its geometry design.

Two approaches are extended in order to validate this simple model:

The purpose of the first part is to apply as boundary conditions, the data provided by a mathematical study realized by J.T. Conway. The interest is to check if it is possible to input the initial conditions in commercial CFD code Fluent 5.5 and compare the results obtained with the mathematical ones. In fact, the different velocities above and below have to be evaluated in order to validate the model.

The second approach is more ambitious because a FORTRAN program is created in order to predict the thrust and tangential forces on each blade. The predicted data will then be implemented within the CFD code Fluent 6.1. Eventually, an evaluation and a validation of this new model is done.

Whatever the approach, the purpose is to obtain a simple method that enables the simulation of the flow induced by helicopter rotor in hover flight. If this methodology is approved, it should be easy to apply to other cases.

Résumé

La finalité de ce stage est de développer une méthode de simulation numérique qui simplifierait la modélisation des écoulements induits par les rotors d'hélicoptères en vol stationnaire. Le principe premier est de considérer les pâles du rotor principal comme un disque plein duquel des pressions et des vitesses débitantes seraient générées.

Si la méthodologie est approuvée, le modélisateur aura la possibilité de travailler avec un modèle de haute qualité définissant l'écoulement d'air quelque soient le nombre de pâles ou la géométrie de cette dernière.

Deux approches sont abordées afin de valider ce projet :

Le propos de la première partie est d'appliquer en conditions limites, les données fournies par une étude mathématique réalisée par J.T.Conway. L'intérêt est de savoir s'il est possible d'introduire ces conditions dans Fluent 5.5 et de comparer les résultats avec ceux obtenus par la méthode mathématique.

La seconde approche est plus ambitieuse puisque un programme FORTRAN est généré afin de prédire la poussée et les forces tangentielles sur chaque pôle. Les données sont ensuite implantées dans le code commercial Fluent 6.1. Finalement, une évaluation des résultats et leurs validations est faite.

Quelque soit l'approche, le but cette démarche est de créer une méthode simple qui soit capable de simuler l'écoulement induit par les pâles d'un rotor principal d'hélicoptère en vol stationnaire. Si cette méthodologie est approuvée, il devrait être facile de l'employer dans d'autres cas beaucoup plus complexes.

A

First Approach

Comparison of a CFD model – Semi-analytical Method

- 1 -

Fundamentals of rotor aerodynamics: Momentum theory

- Conservation laws of fluid mechanics
- Application to hovering rotor
- Rotor Power
- Pressure variation

- 2 -

Exact actuator disk solutions for non-uniform heavy loading and slipstream
contraction developed by J.T.Conway.

- General problem
- Propellers with slipstream rotation

- 3 -

Data provided by Conway (1998)

- 4 -

First CFD approach of the problem

- 5 -

CFD simulation of the problem

- First grid
- Second grid

Fundamentals of rotor aerodynamics

Momentum theory

Hover is a unique flight condition. Here, the rotor has zero forward speed and zero vertical speed. The rotor flow field is, therefore, axisymmetric. With the measurements of the velocity field near and below a hovering rotor, we can note that the fluid velocity increases smoothly as it is entrained into and through the rotor disk plane. There is no jump in the velocity across the disk, although thrust is produced, so there must be a jump in pressure over the disk. With physical pictures of the hovering rotor flow, it is possible to apply a mathematical solution to this problem. Consider the application of three basic conservation laws (conservation of mass, momentum and energy) to the rotor and its flow field.

This approach is called **momentum theory**, and was first developed by Rankine (1865) for marine propellers. The theory was developed further by Froude (1889) and Betz (1920). The main difference between Rankine and Froude theories is in the treatment of the rotor disk as a series of elementary rings, versus the treatment of the disk as a whole.

Conservation laws of fluid mechanics

In the general approach to the problem, it will be assumed that the flow through the rotor is one dimensional, quasi steady, incompressible and inviscid. Consider an ideal fluid, that is, one that generates no viscous shear between fluid elements. Therefore, induced losses are a sole source of losses in the fluid, with other losses resulting from the action of viscosity being assumed negligible.

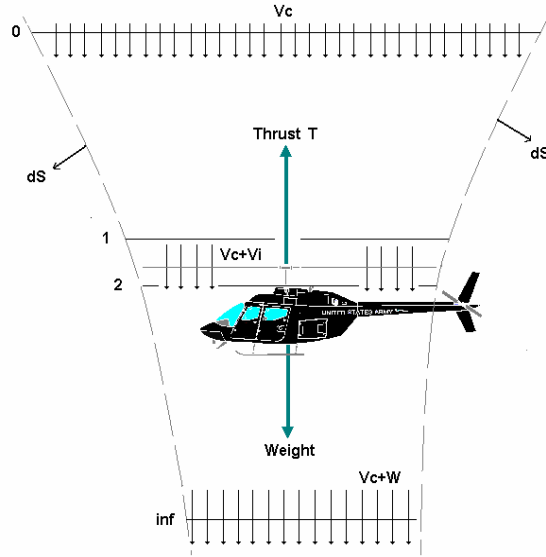


Figure a1: Flow model used for momentum theory analysis of a rotor in axial flight.

A general equation governing the conservation of fluid mass applied to this finite control volume can be written as

$$\oint_S \rho \cdot \vec{V} \cdot d\vec{S} = 0 \quad (\text{eq a.1})$$

Similarly, the conservation of fluid momentum equation can be written as

$$\vec{F} = \oint_S p \cdot d\vec{S} + \oint_S (\rho \cdot \vec{V} \cdot d\vec{S}) \cdot \vec{V} \quad (\text{eq a.2})$$

Thirdly, an equation governing the conservation of energy can be written as

$$W = \oint_S \frac{1}{2} (\rho \cdot \vec{V} \cdot d\vec{S}) \cdot |\vec{V}|^2 \quad (\text{eq a.3})$$

Application to hovering rotor

These general equations of fluid mass, momentum, and energy conservation may now be applied to the specific problem of a hovering rotor. This corresponds to the condition $V_c=0$ on figure a1, the velocities are V_i at the plane of the rotor and W in the far wake. The principle of conservation of mass can be applied,

$$\dot{m} = \iint_{\infty} \rho \vec{V} dS = \iint_2 \rho \vec{V} dS \quad (\text{eq a.4})$$

The principle of conservation of fluid momentum gives the relationship between the rotor thrust T , and the net time rate of change momentum out of the control volume (Newton's second law),

$$\vec{F} = T = \iint_{\infty} \rho(\vec{V} d\vec{S}) \cdot \vec{V} - \iint_0 \rho(\vec{V} d\vec{S}) \cdot \vec{V} \quad (\text{eq a.5})$$

Because in hovering flight, the velocity well upstream of the rotor is quiescent, the second term is zero,

$$T = \iint_{\infty} \rho(\vec{V} d\vec{S}) \cdot \vec{V} \quad (\text{eq a.6})$$

$$T = \dot{m} \cdot w \quad (\text{eq a.7})$$

From the principle of conservation of energy, the work done on the rotor is equal to the gain in energy of the fluid per unit time. The power consumed by the rotor is P and this results in the equation,

$$P = \iint_{\infty} \frac{1}{2} \rho(\vec{V} d\vec{S}) \cdot \vec{V}^2 - \iint_0 \frac{1}{2} \rho(\vec{V} d\vec{S}) \cdot \vec{V}^2 \quad (\text{eq a.8})$$

$$P = \iint_{\infty} \frac{1}{2} \rho(\vec{V} d\vec{S}) \cdot \vec{V}^2 \quad (\text{eq a.9})$$

$$P = \frac{1}{2} \dot{m} \cdot w^2 \quad (\text{eq a.10})$$

Rotor Power

It has been shown previously that momentum theory can be used to relate the rotor thrust to the induced velocity at the rotor disk by using the equation

$$T = \iint_{\infty} \rho(\vec{V} d\vec{S}) \cdot \vec{V} = \dot{m} \cdot w = 2 \cdot \rho \cdot A \cdot v_i^2 \quad (\text{eq a.11})$$

So, the power required to hover is given by

$$P = T \cdot v_i = \frac{T^{3/2}}{\sqrt{2\rho A}} \quad (\text{eq a.12})$$

$$P = 2 \cdot \rho \cdot A \cdot v_i^3 \quad (\text{eq a.13})$$

This power, called ideal power, is entirely induced in nature because the contributions of viscous effects have not been considered in the present level of analysis.

Pressure variation

The pressure variation through the rotor flow field in the hover state can be found from the application of Bernoulli's equation along the streamline above and below the rotor disk. This equation cannot be applied across the disk, because the pressure jump is a result of energy addition by the rotor.

$$p_0 = p_{\infty} = p_1 + \frac{1}{2} \rho \cdot v_i^2 \quad (\text{eq a.14})$$

Below the disk, between 2 and ∞ , the application of Bernoulli's equation gives

$$p_2 + \frac{1}{2} \rho \cdot v_i^2 = p_{\infty} + \frac{1}{2} \rho \cdot w^2 \quad (\text{eq a.15})$$

So, one can write

$$\Delta p = p_2 - p_1 = \frac{T}{A} \quad (\text{eq a.16})$$

The momentum method has permitted a preliminary evaluation of rotor performance in hover. Despite this advantage in providing an insight into the basic theory of the rotor problem, it has many limitations. For example, it provides no information about the distribution of load over the blade. That is the reason why some people are currently developing mathematical theories about heavily loaded actuator disk with non-uniform loading.

- 2 -

Exact actuator disk solutions for non-uniform heavy loading and slipstream contraction developed by J.T.Conway.

(J. Fluid Mech. (1998) Vol. 365, pp 235-267)

A semi analytical method has been developed to solve for the inviscid incompressible flow induced by a heavily loaded actuator disk with non-uniform loading. This method is an extension of the analytical theory of Conway (1995) for the linearized actuator disk and is exact for an incompressible perfect fluid.

General problem

In a recent publication in 1995, Conway derived analytical solutions for the entire flow field induced by a linearized actuator disk with essentially arbitrary radial load distribution. The method was based on the construction of the velocities and vector potential of the ring vortex as integrals over the allowed values of the separation constant of the solutions of Laplace's

equations in cylindrical coordinates. The velocities calculated by this method were finite and continuous everywhere.

The purpose of the article dated on 1998, is to present the extension of this method to the generalised nonlinear actuator disk, subject to the important restriction that the vortex density in the slipstream remains bounded.

Propellers with slipstream rotation

This case will be studied with a commercial CFD code. These results will be applied on the disk later with the set boundary conditions.

The whole mathematical theory is available in the Journal of Fluid Mechanics. To summarise this article without going into too much detail, it provides three velocity profiles in different points above and below the heavy disk. So, it would be possible to know if the numerical calculations made with “Fluent 5.5” and “Fluent 6.0” give results close in comparison to the mathematical predictions.

- 3 -

Data provided by Conway (1998)

In his article published in 1998, J.T.Conway gives the profiles of axial velocity $V_z(r,z)$, of radial velocity $V_r(r,z)$ and azimuthal (or tangential) velocity $V_\theta(r,z)$. However, the paper does not specify the equation curves. So, coordinate points are taken from the paper, which are interpolated.

On the figures a2, a3 and a4, the red lines are the interpolations; a visual comparison of the results approximations with the curves taken from the Journal of Fluid Mechanics can be interesting .

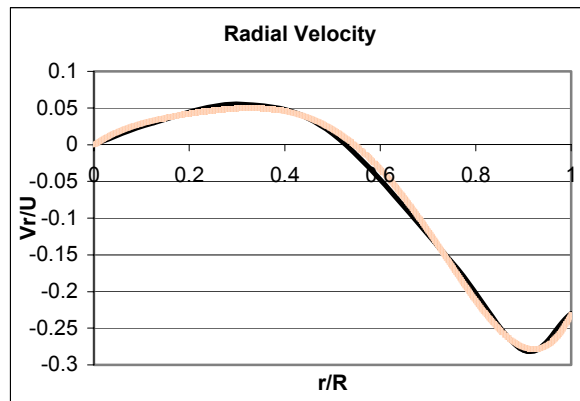


Figure a2: Radial velocity profile as function of the radial coordinates r normalised on the rotor.

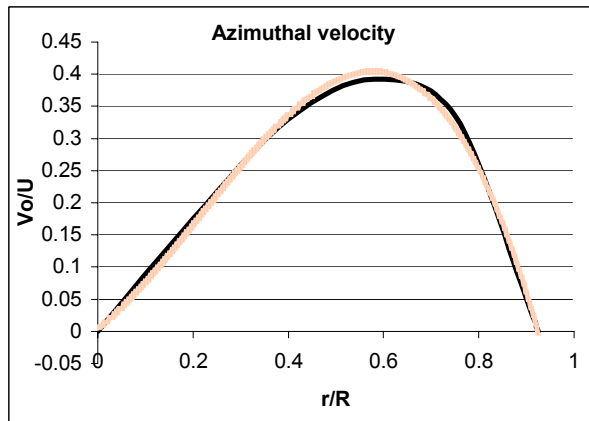


Figure a3: Azimuthal velocity profile as function of the radial coordinates r normalised on the rotor.

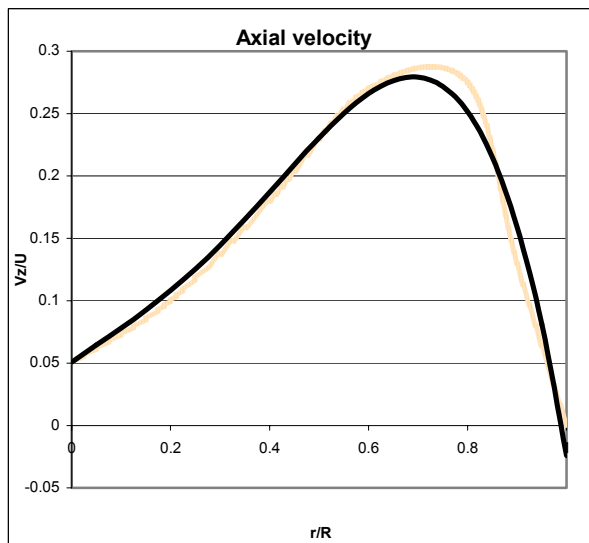


Figure a4: Axial velocity profile as function of the radial coordinates r normalised on the rotor.

Choosing a right order of approximation is difficult. This is why several interpolation orders are used to conserve the best profile.

With this mathematical work, the information needed (i.e. equations) are available; the equations are:

Axial velocity

$$\left| \frac{V_z}{U} \right| = -1.9033*(r/R)^4 + 1.8453*(r/R)^3 - 0.3065*(r/R)^2 + 0.2897*(r/R) + 0.0507$$

Azimuthal velocity

$$\left| \frac{V_\theta}{U} \right| = -1.5006*(r/R)^2 + 1.4972*(r/R) + 0.0018$$

Radial velocity

$$\left| \frac{V_r}{U} \right| = 6.4961*(r/R)^5 - 12.301*(r/R)^4 + 7.3631*(r/R)^3 - 2.2472*(r/R)^2 + 0.4579*(r/R) - 0.0008$$

It is possible to write that the velocity profiles are polynomial equations:

$$\left| \frac{V_z}{U} \right| = \sum_{j=0}^4 A_j \left(\frac{r}{R}\right)^j$$

$$\left| \frac{V_\theta}{U} \right| = \sum_{j=0}^2 B_j \left(\frac{r}{R}\right)^j$$

$$\left| \frac{V_r}{U} \right| = \sum_{j=0}^5 C_j \left(\frac{r}{R}\right)^j$$

j	A _j	B _j	C _j
0	0,0507	0,0018	0,0008
1	0,2897	14,972	0,4579
2	-0,3065	-15,006	-2,2472
3	1,8453	-	73,631
4	-1.9033	-	-12,301
5	-	-	64,961

First CFD approach of the problem

To solve this problem with the Fluent commercial code, it is necessary to specify in the CFD code the azimuthal and radial velocities, and the jump of pressure but the pressure jump equation is not known. For this, the first CFD case is created with a real disk to obtain the total pressure.

It is assumed that there is no interaction between the flow above the disk and the flow below the disk if the total pressure is solved infinitely close to the disk.

In order to apply the velocity profiles, a program in C language (called User Defined Functions) is created.

Making a complex grid of this geometry is not necessary, except near the rotor disk. As a result, the pressure profile is solved for the next simulation. The curve equation is obtained with a sixth order interpolation.

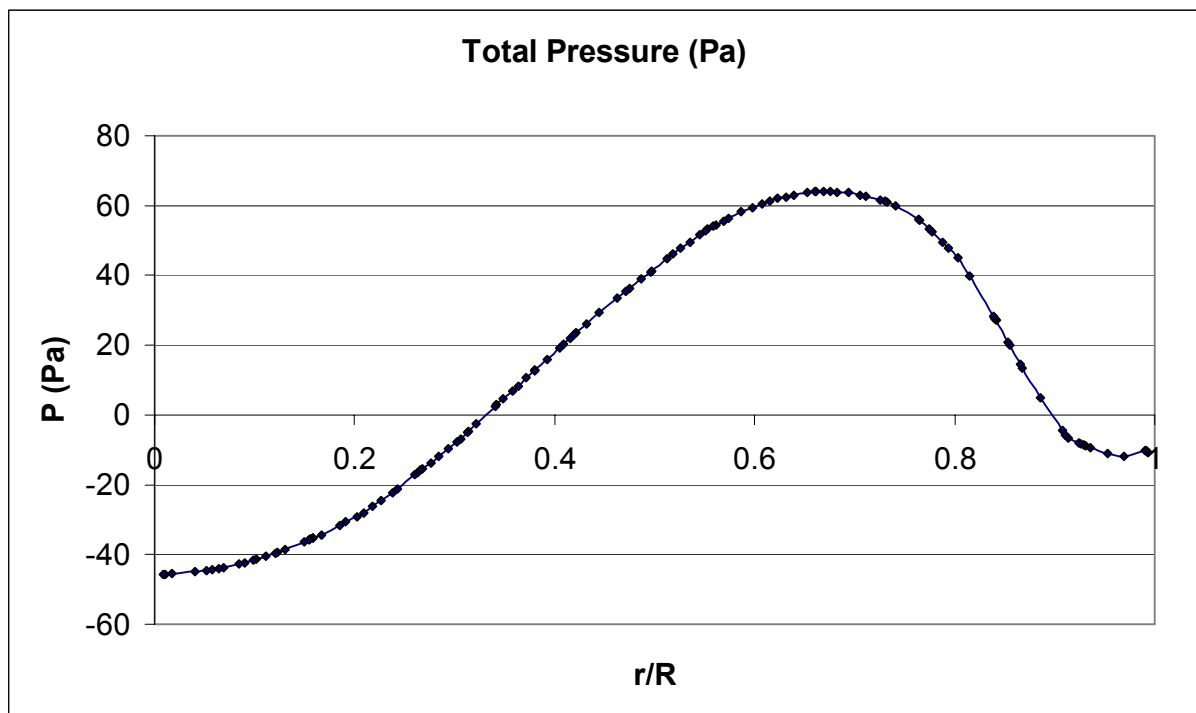


Figure a5: Example of Total pressure profile as function of the radial coordinates r normalised on the rotor calculated with Fluent.

CFD simulation of the problem

The geometry is quite simple because there is only a disk (without thickness) in a square domain. The only difficulty is limiting the size of the domain (for the reason that the meshes would be too numerous) but it cannot be too small (because no interaction with the boundaries would exist).

First grid

The first mesh is not adapted to this case. It assumes that the most important study zone is below the disk. That is why the smallest meshes are in this region and the mesh size increases progressively. It is essential to note that a lot of adapted grids have been tested to observe their differences and their defaults and to increase accuracy. The number of unstructured meshes comes to nearly 415 000.

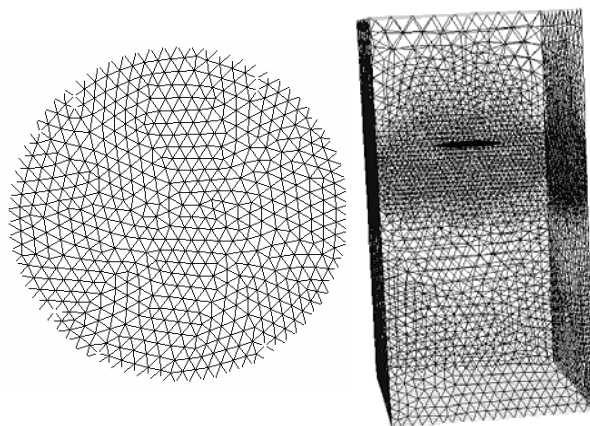


Figure a6 : triangular meshes on the rotor and tetrahedral meshes in the domain.

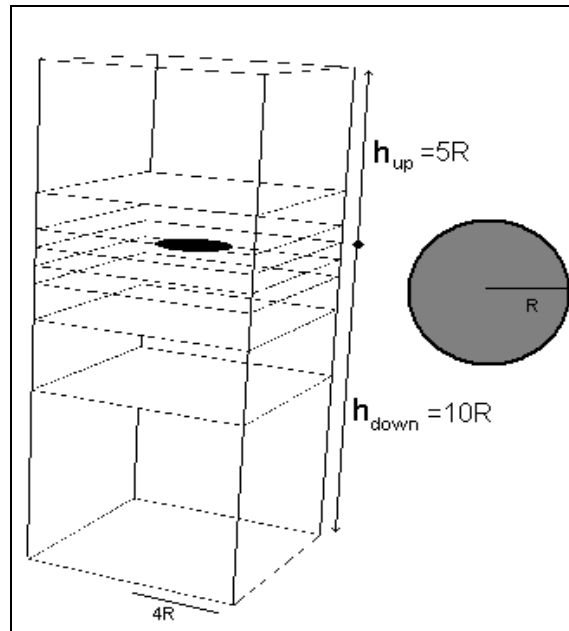


Figure a7: Geometry

The SIMPLE algorithm is used for the pressure-velocity coupled equation and the powerlaw algorithm for the Momentum equations.

The material set is air with a viscosity of $1,7894 \cdot 10^{-5}$ kg/m.s and a density of $1,225$ kg.m⁻³.

The viscous model is the k- ϵ model standard because it provides good curve convergence.

The segregated solver is used in order to solve the V_z , V_r , and V_θ momentum equations.

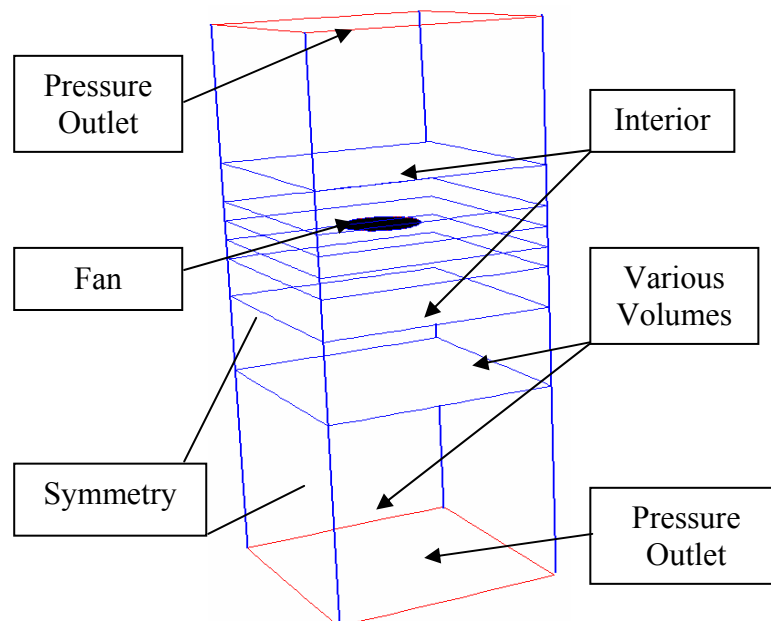


Figure a8: Boundary conditions

Results and discussion

The advantages are:

- The boundary conditions on the disk provide good approximations.
- There is no interaction between the flow induced by the rotor and the limit of the domain.

The disadvantages are:

- Convergence is difficult because a lot of iterations are necessary.
- The convergence criterion is 10^{-3} because better results are really impossible to obtain with this grid.
- The Pressure under-relaxation factor is changed to obtain better convergence.

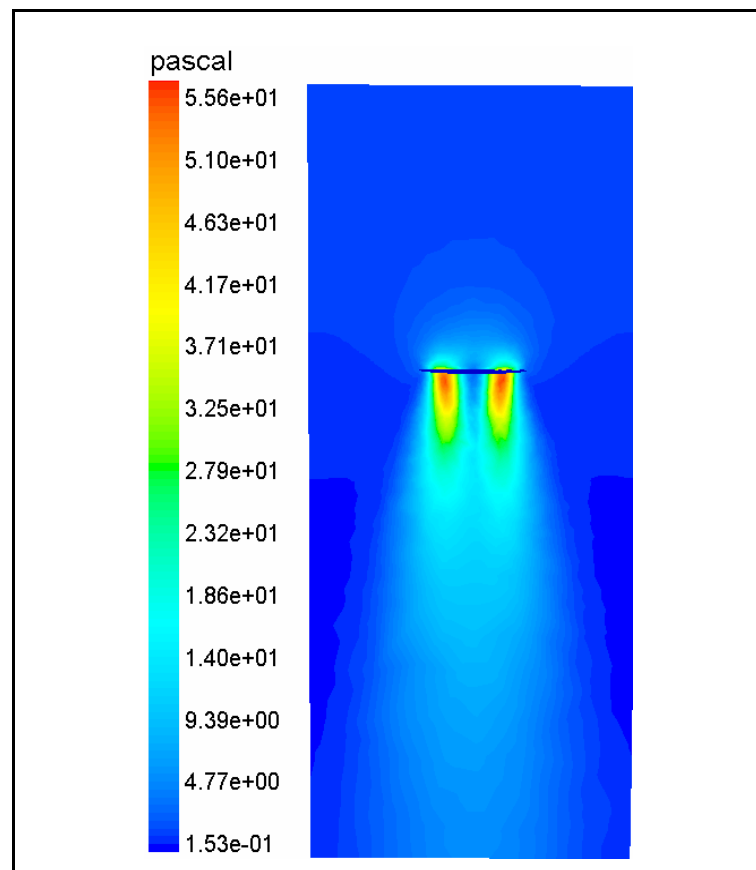


Figure a9: Contour of Dynamic Pressure on a plane

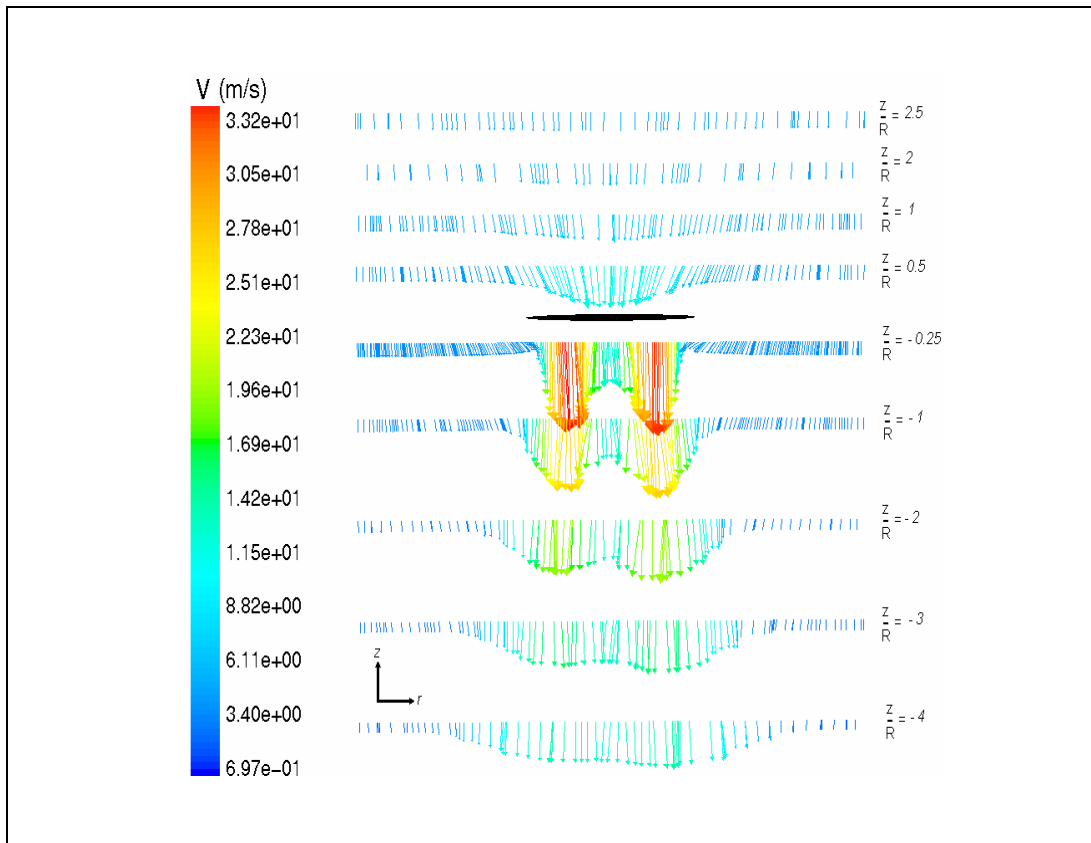


Figure a10: Velocity vectors (on the lines) coloured by Velocity magnitude

Second grid

Another grid is used in order to know what differences result; To control the mesh generation, thirty-three volumes are created. All the interfaces between the two volumes are declared “interior faces” so as too not interfere with the flow.

The number of cells produced is nearly 215000. The boundary conditions, viscous model (k- ϵ model standard) and algorithms are similar to the previous case.

It is important to note that the number of nodes on the rotor is increased after 500 iterations (with “hanging nodes menu” in Fluent) to obtain accuracy values on the rotor.

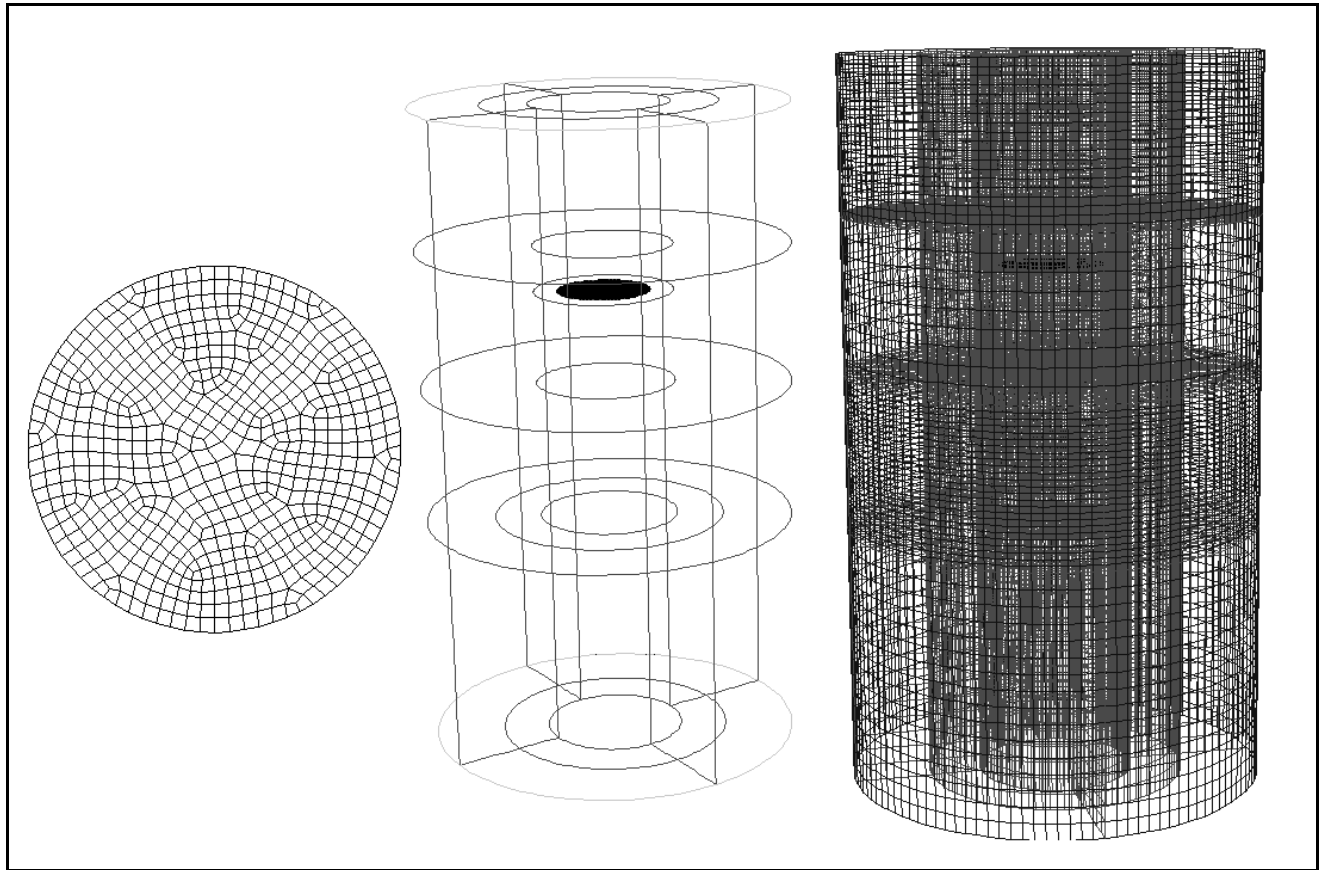


Figure a11: Mesh on the rotor (Quad)

Figure a12: Volumes

Figure a13: Grid

Results and discussion

As it is possible to see on figure a14, the curves of convergence seem to be very good and the convergence criterion is lower than all the previous cases, which have been tested.

The thrust calculated is about 1000 Newton. That infers that, if the helicopter is in hover flight, a helicopter weight of 100Kg is expected.

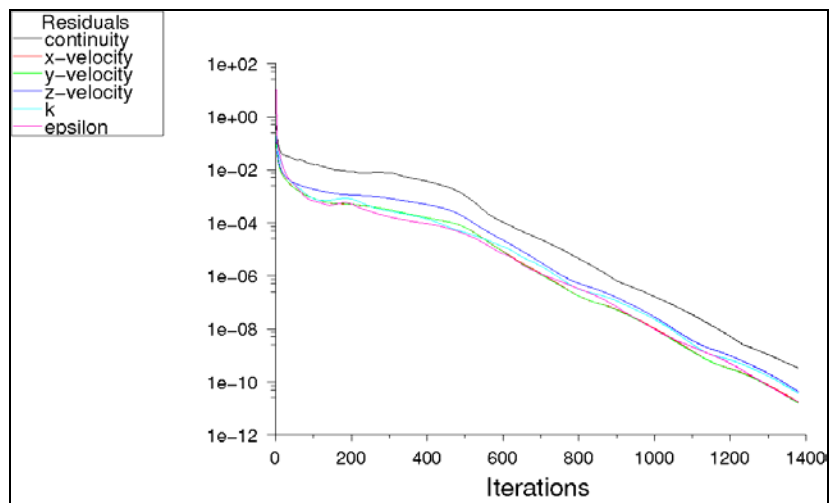


Figure a14 : Scaled residual

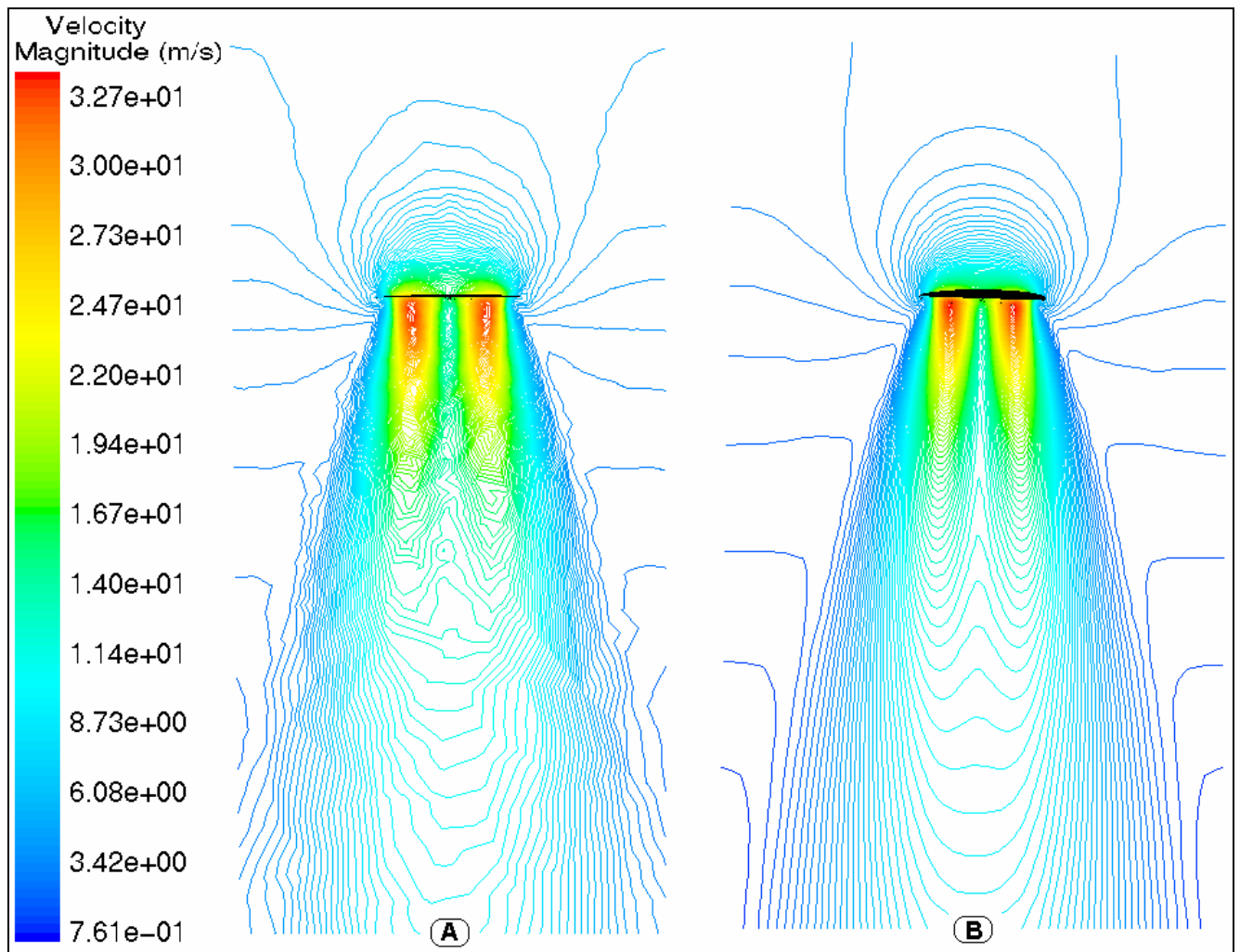


Figure a15: Differences between the first mesh (A) and the second one (B) ;
 Visualization and Comparison of the contour of velocity magnitude on a plane

The boundary conditions on the disk gives good approximations. Checking the curves for jump of pressure on the rotor verifies the initial conditions. With this new cylindrical domain and its quadrilateral mesh, the convergence criterion is $3,4 \cdot 10^{-10}$.

It is obvious from the results to say (observing the figure a15 about contour of velocity magnitude) that the second grid provides more accurate results. The results are similar to a numerical study made by the AIAA with another adapted Navier-Stokes CFD code after grid adaptation to this case.

Furthermore, this new mesh provides smooth visualisation, which corresponds to the reality of rotor aerodynamics.

On figure a15.A, the contour of velocity magnitude depends of the number and especially the node shapes. In opposition to this problem, the second mesh provides results independent of the grid.

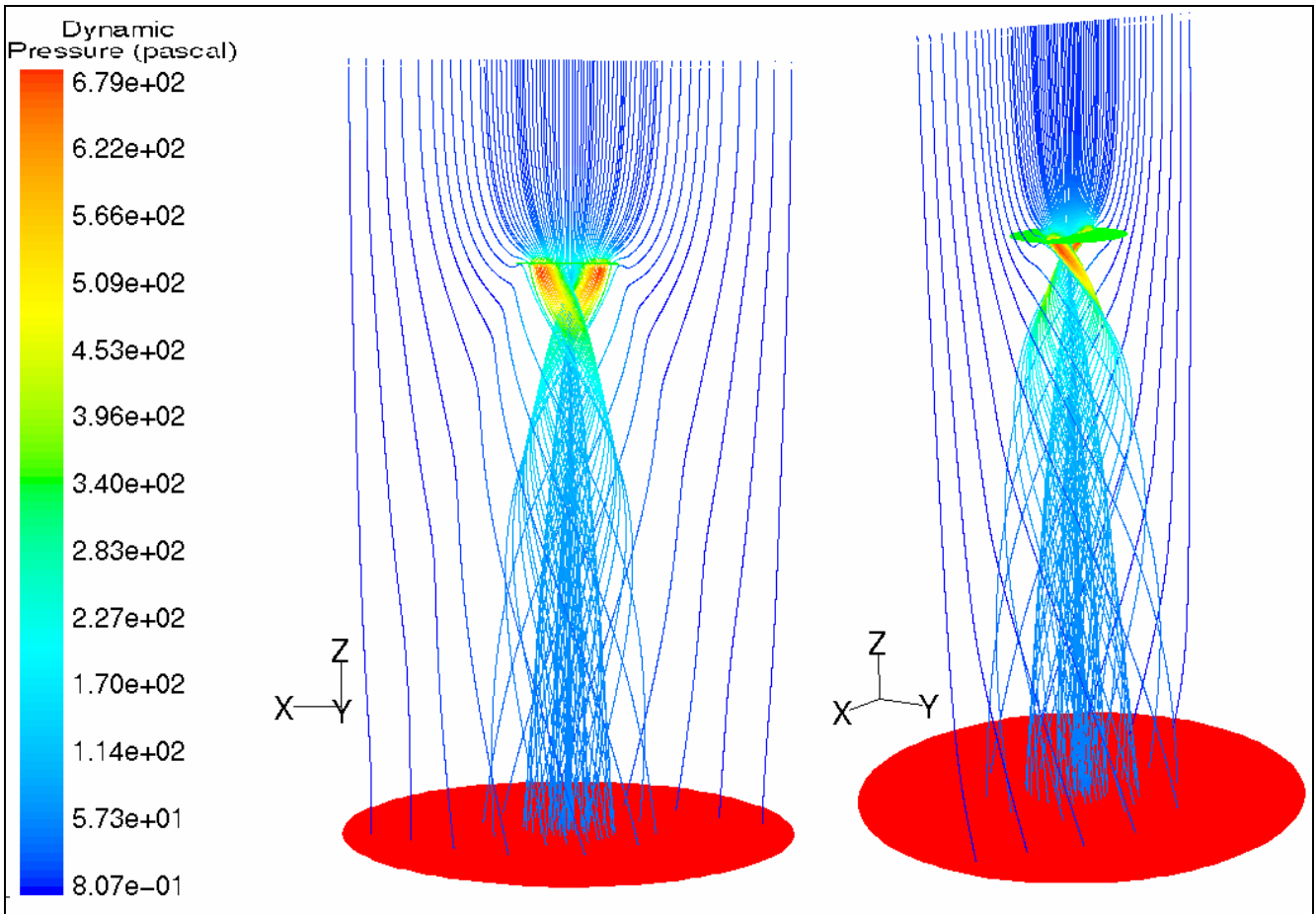


Figure a16: pathlines coloured by dynamic pressure

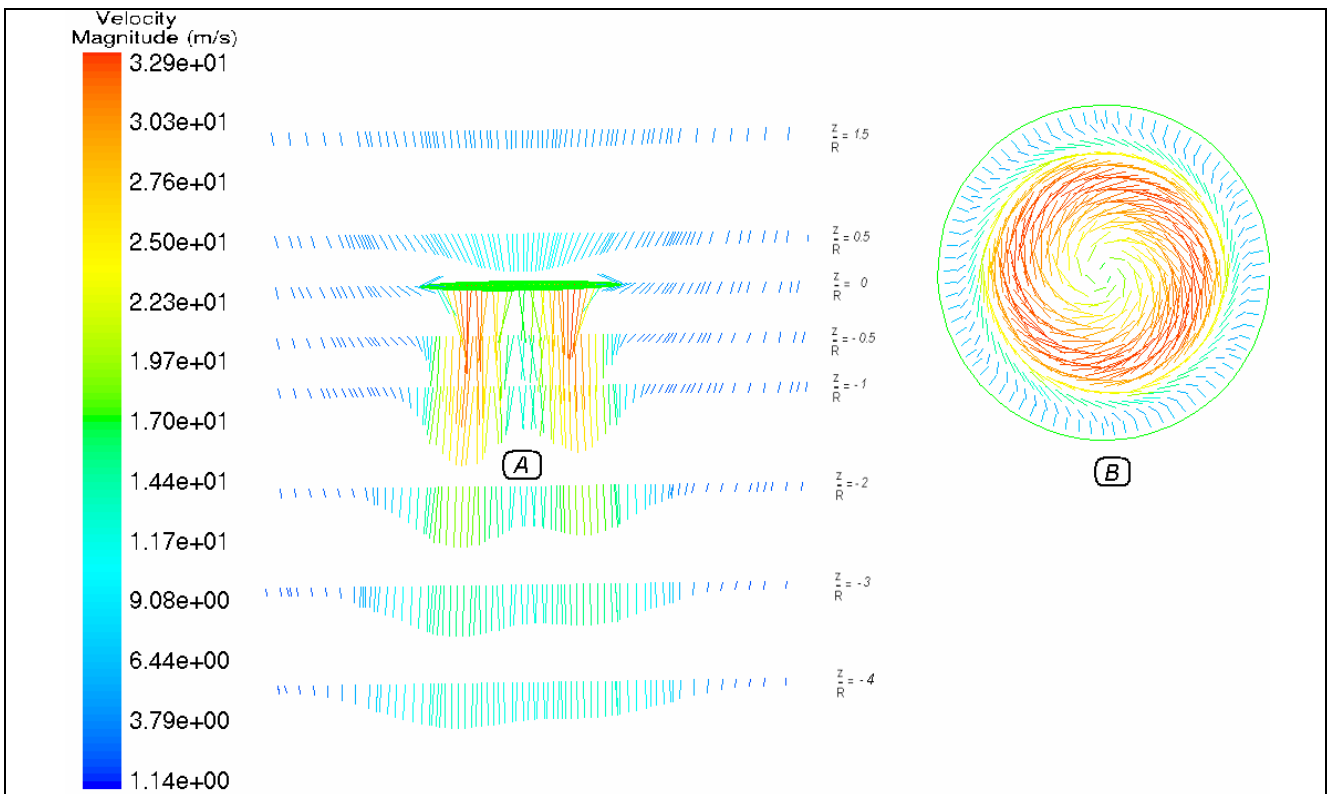


Figure a17: Velocity vectors on X-lines (A) and on the disk (B) coloured by Velocity magnitude

Figure a16 shows the pathlines taken by the dynamic pressure. When the flow goes through the disk, the particle velocity increases. In addition to the acceleration phenomenon, a vortex is generated by the rotor.

It is noted that the flow velocity increases before the rotor, but the jump of velocity (induced by the actuator disc model) provides accurate values.

Figure a17.A provides information about the velocity vectors on different lines above and below the rotor. The rotor draws in the flow and accelerates it. Below the disk, it is easy to observe the vortex generation (with figure a17.B) and to note that the velocities are very low:

- in the middle of the disc,
- and close to the boundary of the disc.

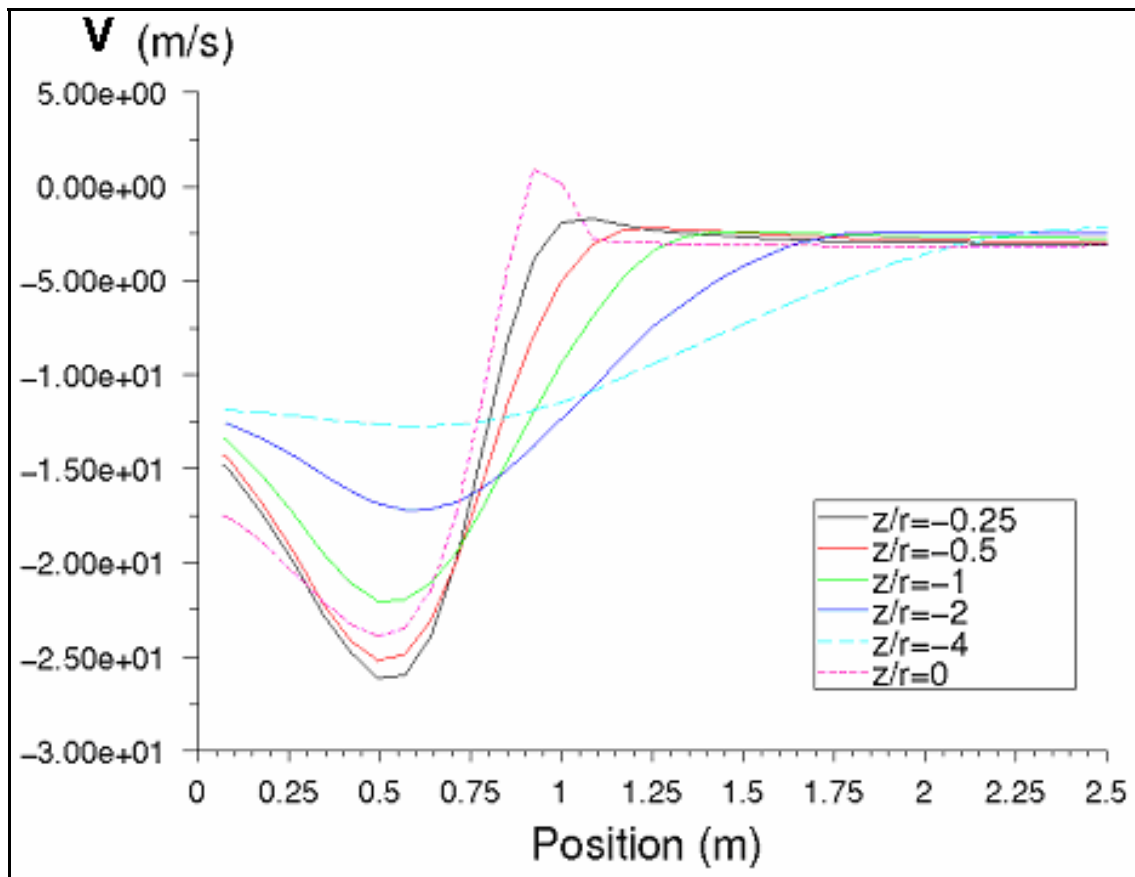


Figure a18: axial velocity profiles below the rotor as function of the radial coordinates r normalised

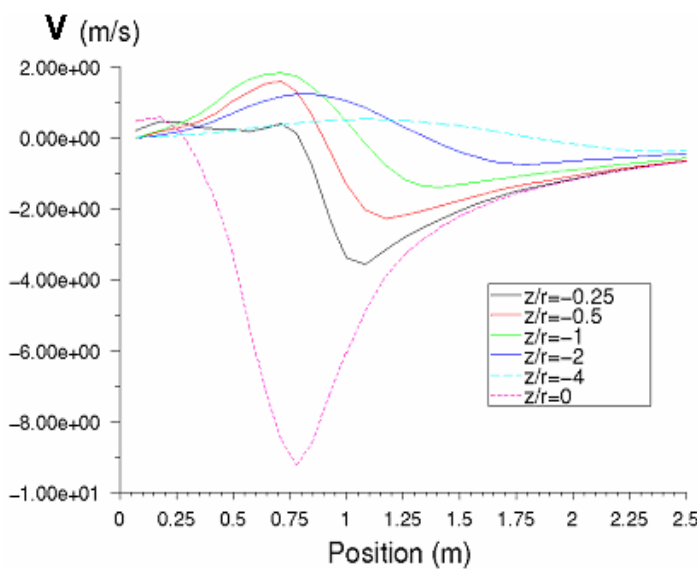


Figure a19: radial velocity profiles below the rotor as function of the radial coordinates r normalised

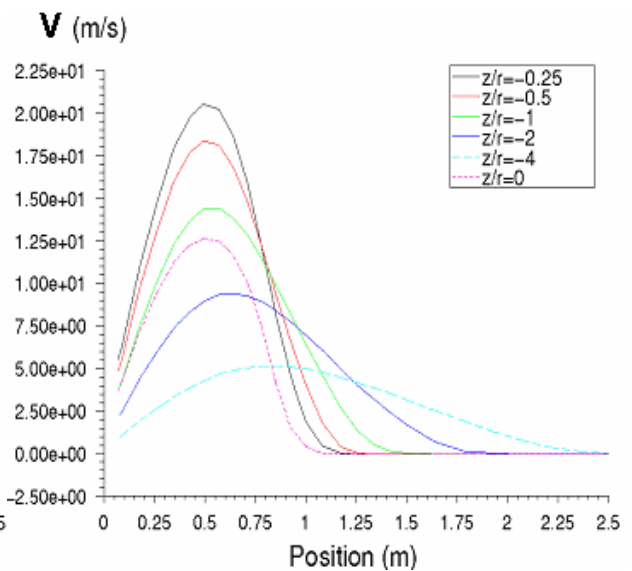


Figure a20: tangential velocity profiles below the rotor as function of the radial coordinates r normalised

Figures a18, a19 and a20 show the different velocity profiles as a function of the radius at different z coordinates. Considering the axial velocity, the results are not similar to Conway's, especially after the coordinate $\frac{z}{R} = -1$. It is not surprising because the analytical method used in his work is so different than the one proposed by the CFD commercial code Fluent 5.5.

To summarise, three velocity profiles and one jump pressure profile must be applied. Even if applying the velocities and pressure values required is not simple, a good approximation can be made in order to obtain the right thrust value.

For this example:

The mass flow rate provided by the rotor is:

$$\dot{m} = 50.467 \text{ kg/s}$$

The velocity magnitude integral on the rotor is:

$$\iint_{\Omega} \vec{V} \, dS = 61.43 \text{ m}^3 \cdot \text{s}^{-1}$$

$$V_{\text{average}} = \frac{61.43}{S}$$

$$V_{\text{average}} = 19.55 \text{ m} \cdot \text{s}^{-1}$$

An approximation of the thrust induced by the rotor is given as:

$$T = \dot{m} \cdot V_{\text{average}}$$

T= 986.82 N

In hover flight, the weight of the helicopter should be approximately 100,59 kg. In order to know with accuracy this weight, it would be insightful to introduce the fuselage and its characteristics (like the vertical drag C_{Dv}) in the calculation.

A real rotor would give a higher thrust value. For this, if CFD simulations should be realised in the future, the jump of pressure will be more realistic but the velocity profiles should be identical.

Even if the CFD calculations do not provide perfect and expected results, knowledge has been developed in order to, in the next chapter, obtain a complete study.

B

Second Approach

“Blade Element Momentum (BEM)” and “CFD” coupled Calculations for Helicopter in Hover Flight

1. Theoretical work

1.1. Actuator disc model

1.2. Blade Element Theory

2. Programme generation

2.1. Algorithm

2.2. Subroutine

2.3. Structure of the programme

3. Results and discussion

4. Data implementation in FLUENT

4.1. Implementation

4.2. Geometry and Meshes

4.3. Numerical Procedure

4.4 Results and discussion

- *Validation with the total pressure and thrust*
- *Streamlines functions*
- *Dynamic Pressure on the disc*
- *Velocity profiles*
- *Velocity on the z-axis*

The main interest of this part is to develop a FORTRAN programme in order to obtain the Thrust and Tangential forces distribution. From this, It is possible to implement these Forces in the CFD commercial code FLUENT via the *Actuator Disc Model*, with the purpose to determine the flow induced by this modeling method.

Various methods can be used to calculate the aerodynamic forces acting on the blades of a wind turbine. The most advanced is numerical methods solving the Navier-Stokes equations for the global compressible flow as well as the flow near the blades. The two major approaches to calculate the forces are the *Actuator Disc Model* and the *Blade Element Model*. In the following sections, a brief introduction of both mentioned methods are presented.

1. Theoretical work.

This theoretical part is a summary of a thesis written by Anders Ahlström, entitled “Simulating Dynamical Behaviour of Wind Power Structures” (Royal Institute of Technology Department of Mechanics, in Stockholm (2002)). The introduction focus on the qualitative results and the basic assumptions that are made.

1.1. Actuator disc model

The actuator disc model is based on Bernoulli’s equation and energy balances. It’s assumed that the rotor is replaced by an actuator disc, through which the static pressure decreases discontinuously. The fluid is assumed incompressible.

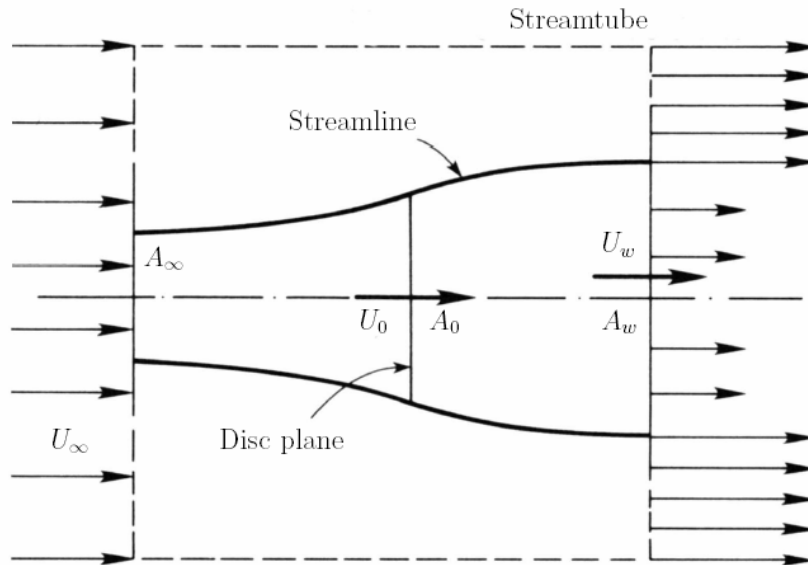


figure b1: Flow pattern inside the streamtube.

The streamtube has a cross-sectional area smaller than the cross-sectional area for the upstream disc and a larger area than the downstream disc. Within the streamtube, continuity is required and the rate of the mass flow must be constant.

$$\dot{m} = |\rho_{\infty} A_{\infty} U_{\infty}| = |\rho_0 A_0 U_0| = |\rho_w A_w U_w| \quad (\text{eq b.1})$$

By introducing an axial interference factor, a , as the fractional decrease in wind velocity between the free stream and the rotor plane represented by

$$a = \frac{v}{U_{\infty}} \quad (\text{eq b.2})$$

with $\begin{cases} U_{\text{inf}} \text{ is the undisturbed air speed} \\ v \text{ is free stream velocity} \end{cases}$

it is found that

$$U_0 = U_{\infty}(1 - a) \quad (\text{eq b.3})$$

The air, which goes through the disc. The velocity multiplied by the flow rate gives the rate of change of momentum, more known as a force

$$T = \dot{m}(U_{\infty} - U_w) \quad (\text{eq b.4})$$

Combining the equations above with the fact that the change of momentum comes entirely from the pressure difference across the actuator disc, it is obtained that

$$p_0^+ - p_0^- = (U_{\infty} - U_w) \cdot \rho_0 \cdot U_{\infty} (1 - a) \quad (\text{eq b.5})$$

To obtain the pressure difference, the Bernoulli's equation is applied separately to the upstream and downstream section of the streamtube. For the upstream section it becomes

$$\frac{1}{2} \rho U_{\infty}^2 + p_{\infty} = \frac{1}{2} \rho U_0^2 + p_0^+ \quad (\text{eq b.6})$$

Similarly, for the downstream

$$\frac{1}{2} \rho U_w^2 + p_{\infty} = \frac{1}{2} \rho U_0^2 + p_0^- \quad (\text{eq b.7})$$

Subtracting (eq b.7) from (eq b.6) yields

$$p_0^+ - p_0^- = \frac{1}{2} \rho (U_{\infty}^2 - U_w^2) \quad (\text{eq b.8})$$

As the fluid is incompressible, Equation (eq b.8) and (eq b.5) gives

$$U_w = U_{\infty} (1 - 2a) \quad (\text{eq b.9})$$

The force, T , is obtained by substituting (eq b.9), (eq b.3) and (eq b.1) into (eq b.4), which gives

$$T = 2\rho A_0 U_{\infty}^2 a(1 - a) \quad (\text{eq b.10})$$

Combining (eq b.3), (eq b.9) and the rate of work done by the force, $P = T.U_0$, the power extraction from the air is obtained as

$$P = 2\rho A_0 U_\infty^3 a(1-a)^2 \quad (\text{eq b.11})$$

or, by introducing the dimensionless power-coefficient, $C_p = a(1-a)^2$

$$P = 2\rho A_0 U_\infty^3 C_p \quad (\text{eq b.12})$$

The power-coefficient represents the efficiency of the turbine, which depends on variables like the wind speed, the rotor speed and the pitch angle. The coefficient shows how much of the kinetic energy in the air stream that is transformed into mechanical energy.

1.2. Blade Element Theory

While using of aero elastic codes in design calculations, the aerodynamic method has to be efficient CPU time. The Blade Element Momentum (BEM) theory, has been shown to give good accuracy with respect to time cost.

In this method, the turbine blades are divided into a number of independent elements along the length of the blade. At each section, a force balance is applied involving 2D section lift and drag with the thrust and torque produced by the section. At the same time, a balance of axial and angular momentum is applied. This produces a set of non-linear equations, which can be solved numerically for each blade section.

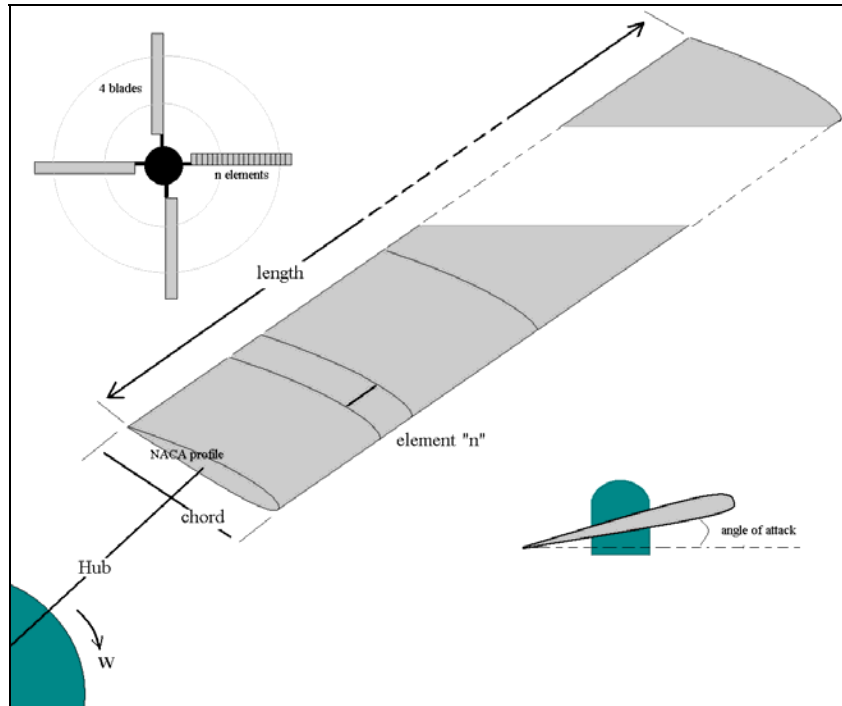


Figure b2: problem description

In Section “1”, only the force in the flow direction was considered. The BEM theory also takes notice of the tangential force due to the torque in the shaft. The lift force L per unit length is perpendicular to the relative speed V_{rel} of the wind and equals

$$L = \frac{\rho c}{2} V_{rel}^2 C_L \quad (\text{eq b.13})$$

Where C_L is the lift coefficient.

Where c is the blade cord length. The drag force D per unit length, which is parallel to V_{rel} is given by

$$D = \frac{\rho c}{2} V_{rel}^2 C_D \quad (\text{eq b.14})$$

Where C_D is the drag coefficient.

Since we are interested only in the forces normal and tangential to the rotor-plane, the lift and drag are projected in these directions

$$F_N = L \cos \varphi + D \sin \varphi \quad (\text{eq b.15})$$

And

$$F_T = L \sin \varphi - D \cos \varphi \quad (\text{eq b.16})$$

The theory requires information about the lift and drag aerofoil coefficients C_L and C_D . Those coefficients are generally given as functions of the angle of incidence (see Figure).

$$\alpha = \varphi - \theta \quad (\text{eq b.17})$$

where α is the angle of attack

φ is the angle of the relative velocity

Further, it is seen that

$$\tan \varphi = \frac{(1 - a)U_\infty}{(1 + a')wr} \quad (\text{eq b.18})$$

In practice, the coefficients are obtained from a 2D wind-tunnel test. If α exceeds about 15° , the blade will stall. This means that the boundary layer on the upper surface becomes turbulent, which will result in a radical increase of drag and a decrease of lift. The lift and drag coefficients need to be projected in the same way as the forces F_N and F_T . C_N and C_T are calculated as follow:

$$C_N = C_L \cos \varphi + C_D \sin \varphi \quad (\text{eq b.19})$$

And

$$C_T = C_L \sin \varphi - C_D \cos \varphi \quad (\text{eq b.20})$$

Further, a solidity σ is defined as the fraction of the annular area in the control volume, which is covered by the blades

$$\sigma = \frac{Area_{Blades}}{Area_{Disc}} \quad (\text{eq b.21a})$$

so in the cylinder system of coordinate (r, ψ, z) ,

$$\sigma(r) = \frac{c(r)N}{2\pi r} \quad (\text{eq b.21b})$$

where N denotes the number of blades.

The normal force dT and the torque dQ on the control volume of thickness dr , is since F_N and F_T are forces per length

$$dT = N.F_N.dr = \frac{1}{2} \rho.N \frac{U_\infty^2 (1-a)^2}{\sin^2 \phi} c.C_N dr \quad (\text{eq b.22})$$

and

$$dQ = r.N.F_T.dr = \frac{1}{2} \rho.N \frac{U_\infty .wr.(1-a)(1+a')}{\sin \phi .\cos \phi} c.C_T .r.dr \quad (\text{eq b.23})$$

Finally, the two induction factors are declared by

$$a = \frac{1}{\frac{4 \sin^2 \phi}{\sigma.C_N} + 1} \quad (\text{eq b.24})$$

$$a' = \frac{1}{\frac{4 \sin \phi \cos \phi}{\sigma.C_T} - 1} \quad (\text{eq b.25})$$

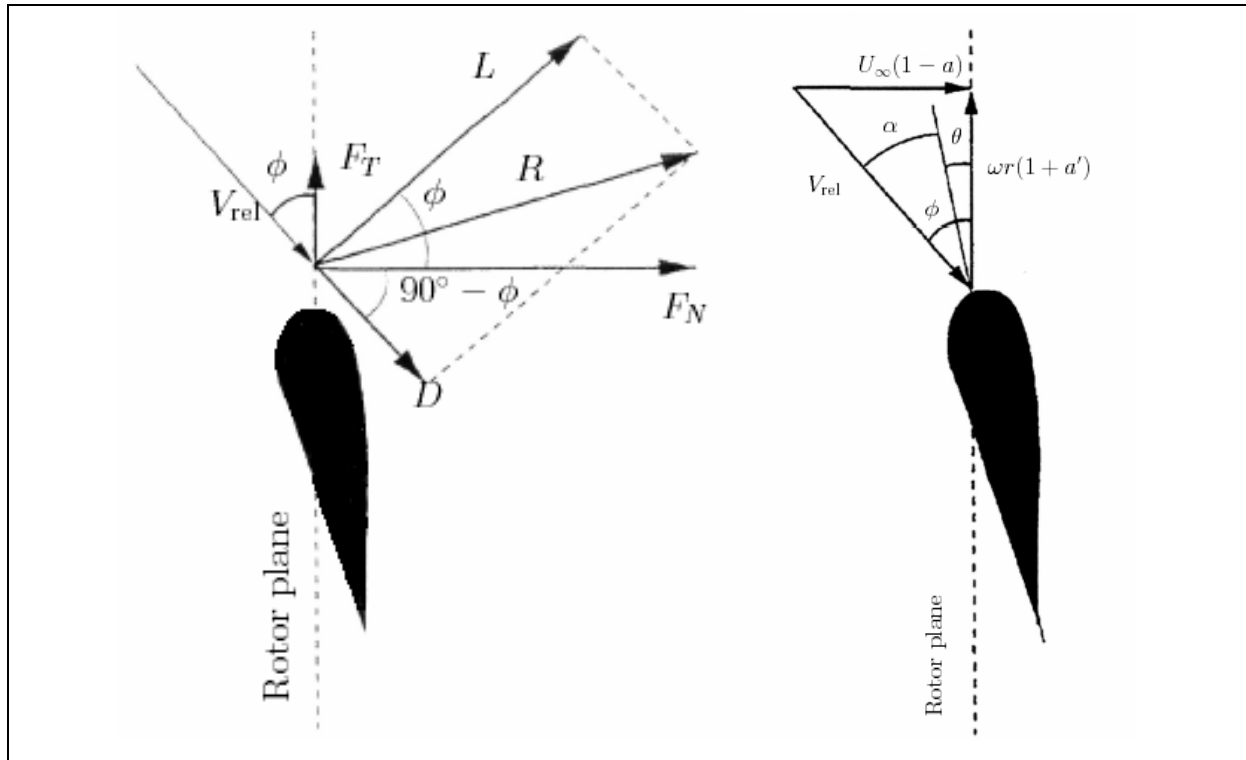


Figure b3: The local forces and velocity components on the blade

2. Programming

2.1. Algorithm

All necessary equations have now been derived for the BEM model. Since the different control volumes are assumed to be independent, each strip may be treated separately and therefore the results for one radius can be computed before solving for another radius.

For each control volume, the algorithm can be divided into eight steps:

1. Initialize a and a' , typically $a_0 = a'_0 = 0$.
2. Compute the flow angle, ϕ , using (eq b.18).
3. Compute the local angle of attack using (eq b.17).

4. Read $C_L(\alpha)$ and $C_D(\alpha)$ from a subroutine.
5. Compute C_N and C_T from (eq b.19) and (eq b.20).
6. Calculate a and a' from (eq b.24) and (eq b.25).
7. If $|a_i - a_{i-1}| < \eta$ and $|a_i' - a_{i-1}'| < \eta$ where η is a tolerance, then stop else go to step 2.
8. Compute the local forces on each element of the blades.

2.2. Subroutine

The main part of this subroutine was written in Fortran77 by Dr James Marchman and his research group (Virginia Polytechnic Institute and State University, USA). The author used his research work to calculate drag and lift coefficients.

The code can work without this subroutine (because the using of C_D and C_L data tables is possible) but choosing the “NACA number” (defining the blade geometry) or the number of pressure nodes are alternatives more interactive and so, more flexible.

Moreover, in the future, when twisted blades are studied, this subroutine will represent the simplest configuration in opposition to multiple Data Tables in many Data files.

This subroutine admits the Classic Hess and Smith Method. A.M.O. Smith at Douglas Aircraft directed an incredibly productive aerodynamics development group in the late '50s through the early '70s. The description of the implementation of the theory given above that originated in his group is available on the Aerospace and Ocean Engineering Department Website (Virginia Polytechnic Institute).

The approach consists in:

- i)* Breaking up the surface into straight line segments
- ii)* Assuming the source strength is constant over each line segment (panel) but has a different value for each panel
- iii)* Assuming that the vortex strength is constant and equal over each panel.

2.2.1. Subroutine principles

The subroutine defines the surface for NACA four or five digit airfoil shapes and automatically places panels on that surface. It gives the chosen airfoil shape and the pressure coefficient distribution.

With the information about the induced angle of attack, it is possible to calculate the pressure coefficients, i.e. the lift and drag coefficients. As it was shown in the first part, the steps of the programme are as following:

1. Data's inputs are the NACA number of the uniform blade, and the induced angle of attack (which is calculated by the main programme).
2. All the nodes of the body shape are solved in order to calculate everywhere the pressure coefficients.
3. Coefficients of linear system are determined.
4. Solutions of linear algebraic system by Gaussian elimination with partial pivoting are found.
5. The pressure distribution is determined.
6. Finally, the lift and drag coefficients are computed. C_d and C_l are input in the main programme.

The above-mentioned steps are followed at each iteration. It is easy to understand that this programme needs a lot of memory for the computer used. That is why a nodes limit will be applied in the future.

2.2.2. Example

In order to show how this subroutine works, an example is made for this configuration:

- NACA number: 23012
- Angle of attack: 6 degrees
- Number of nodes: 90

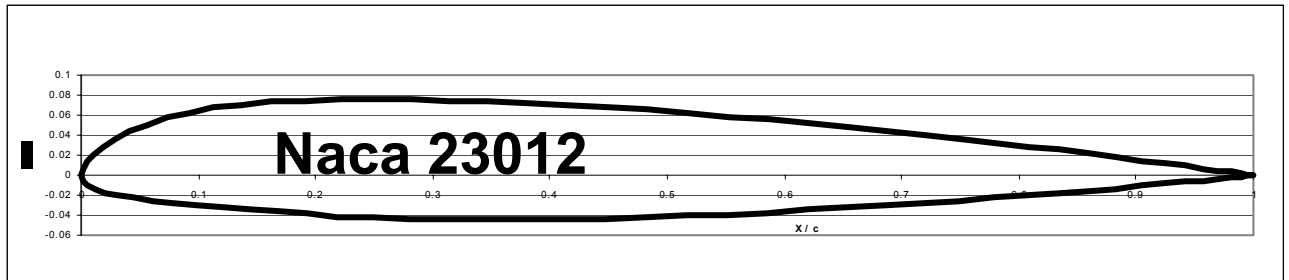


Figure b4: Shape of NACA 23012

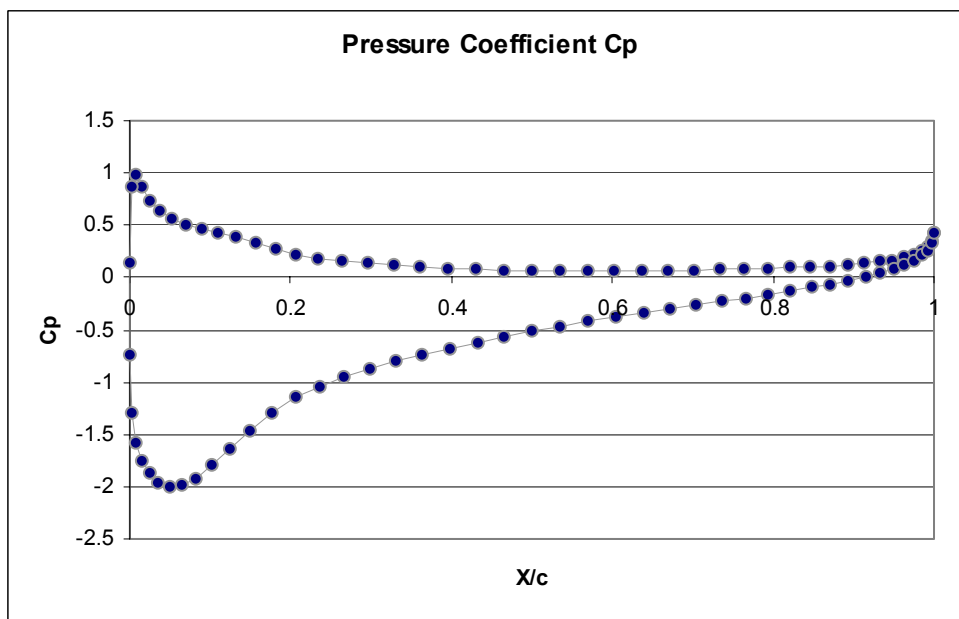


Figure b5: Pressure coefficient on the blade

The results provide the ninety points on the body shape of the bidimensionnal airfoil. As it is possible to see in figure b4, the profile is actually respected.

Curves about repartitions of intrados and extrados C_p are given. Other coefficients are available:

- The lift coefficient is $8,5461.10^{-1}$
- The drag coefficient is $-4,2.10^{-4}$

The interest is not to know the shape or the C_p but the programme needs this data to solve equations and to get C_D and C_L . These coefficients are input in the main programme.

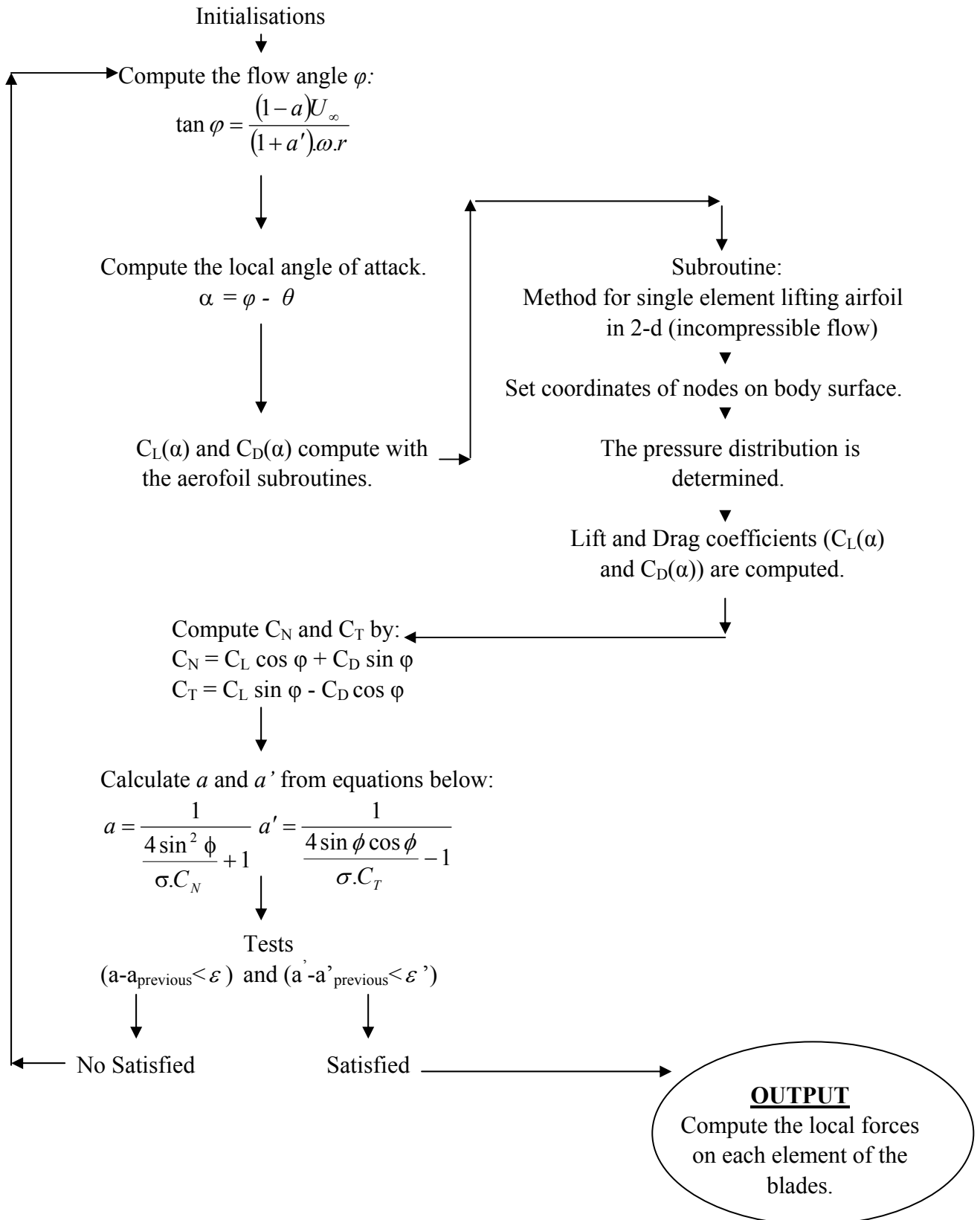
To conclude, it's assumed that this subroutine (which will be integrated in the main programme) works and provides accurate results.

This Smith-Hess panel method for single element lifting airfoil in 2-D incompressible flow will be used in the next chapter but it's admitted that this subroutine is independent of the Reynolds number.

2.3. Structure of the programme

INPUT:

General	Blades characteristics	Blades geometry
Number of Elements	Angle of attack.	NACA number
U_∞	Radial velocity	Chord
	Number of blades	Length
		Hub



The whole programme is available in the appendices with all the explanations about the subroutines.

3. Results and discussion

In the simple momentum theory for an actuator disc, the flow conditions and aerodynamic loads are assumed constant in the azimuthal and radial direction. Furthermore this theory is only valid for lightly loaded discs with an infinite number of blades.

Initial conditions are the same than another CFD study realized by another student from this department.

$\rho = 1,125 \text{ kg.m}^3$	<i>air density</i>
$R_{\text{hub}} = 0,3 \text{ m}$	<i>hub</i>
$\theta = 8 \text{ degrees}$	<i>blade angle of attack</i>
$\omega = 30. \pi \text{ rad.s}^{-1}$	<i>velocity angle</i>
$c = 0,16 \text{ m}$	<i>chord</i>
$n = 4$	<i>number of blades</i>
$\text{Length} = 1,7 \text{ m}$	<i>length of the blades</i>
$U_{\infty} = 35.6 \text{ m.s}^{-1}$	<i>Velocity upstream</i>
$\text{Naca} = 20012$	<i>naca number</i>

Each element has the same size as the other ones. For this case, the blade is non twisted but the inflow ratio is non uniform. Several configurations are performed various number with of elements to define the profiles.

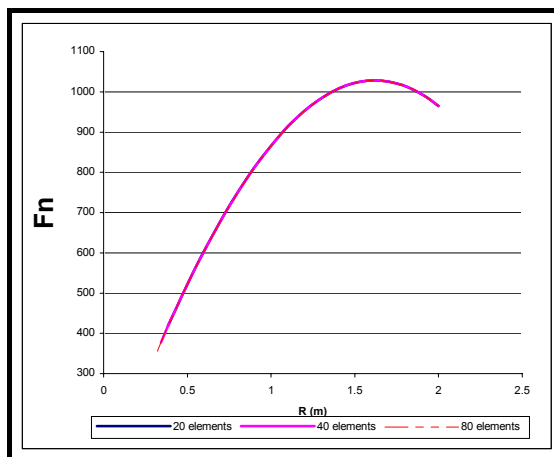


Figure b6: Fn with different numbers of element

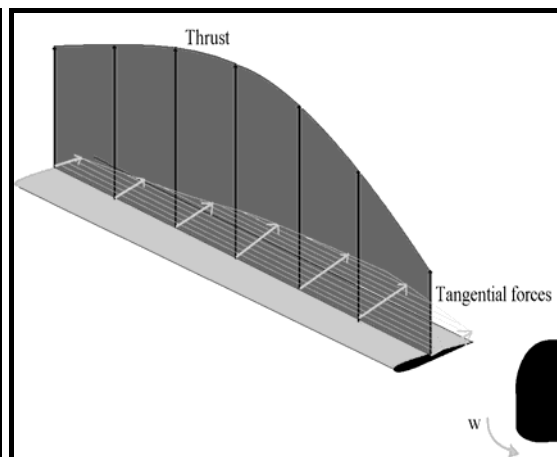


Figure b7: Forces repartition on the blade

The results compared themselves when the numbers of blades changes, in order to check the behaviour of T. Three numbers are tested: 20,40,80.

If the total thrust on the four blades is quantified, it's easy to conclude that the results are quite similar:

For 20 el^t, $T_1 = 5811,749$ N;

For 40 el^t, $T_2 = 5760,633$ N;

For 80 el^t, $T_3 = 5734,453$ N;

It seems that T tends a constant value when the number of element increases. For example, the numerical error between T_1 and T_3 are: 1,33%.

In order to compare the results given by the Fortran programme with another works, the same initial conditions are taken. The number of 60 elements is chosen because it's good alternative between the time and memory costs and the forces repartition accuracy.

So, finding forces repartition on the blade with this FORTRAN programme is now easy. On the figure b8 is shown the thrust and tangential forces with the initial conditions taken here. Figure b7 is only presented to have an idea of normal forces on one blade versus tangential forces induced by the blade rotation around the rotor and not to get a quantitative result.

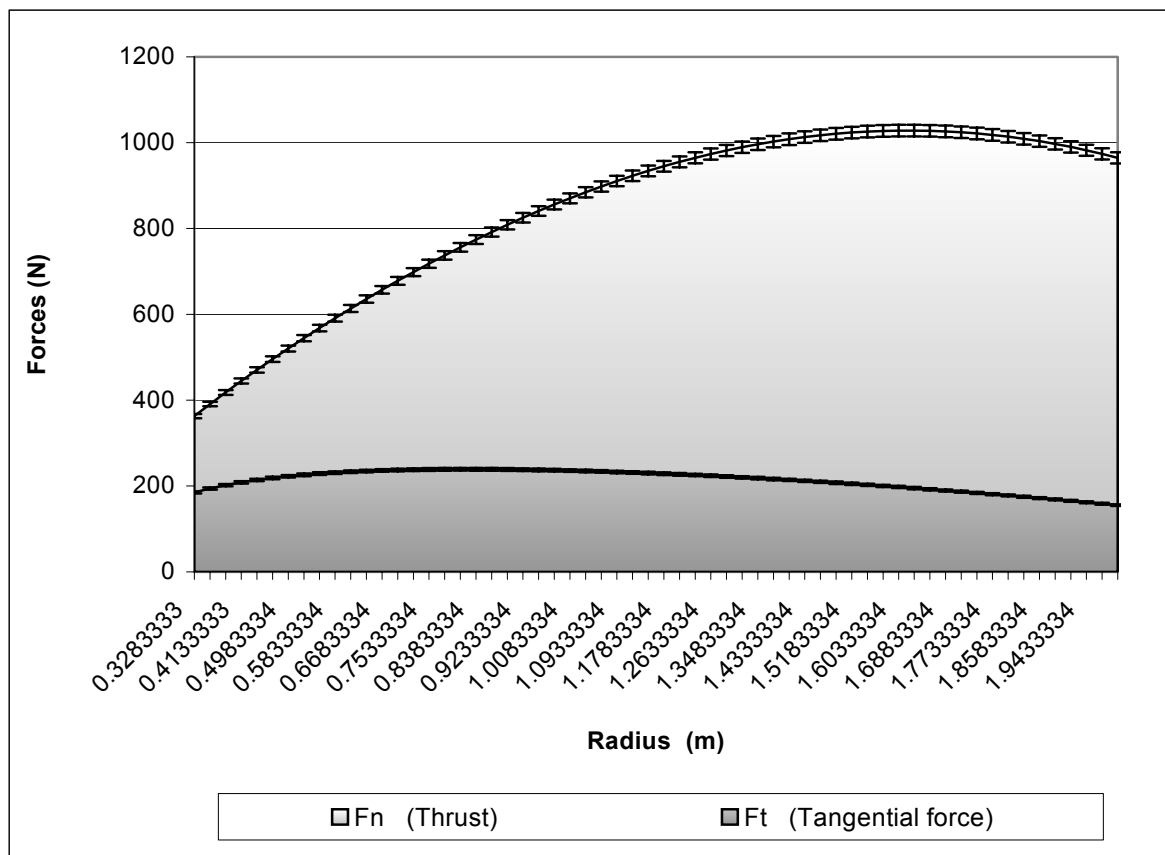


Figure b8: Thrust and tangential force repartitions on the blade

As can be seen on the figure b8, the error bars are very small when it is compared to the tangential forces values. Representative results are revealed that the thrust F_n is bigger than F_t everywhere. Obviously, the NACA profile is studied to provide this effect. The tangential force decreases after 0.6m-Radius in opposition to the thrust, which increases until 1.7 m radius and decreases a little bit at the end of the blade.

Moreover, the thrust is big after 1-meter radius. So, if the blade were divided in two parts, the bigger forces would be on the second one. This problem could damage the rigidity of the blade because there is not a good force repartition. That is the reason why aerodynamicists twist the blade in order to reduce the thrust at the end of the blade. Another way to reduce these too higher forces is to apply flapping angle; indeed, even if it is small (3-6 degrees), the flapping angle represents the balance between the aerodynamic and centrifugal forces.

It is assumed that α is the real angle of attack because it is the difference between ϕ (angle between the velocity vector and the rotor plane) and the basic angle of attack θ (8 degrees in this case). $\alpha(r)$ decreases when the radius r increases. The angle of attack is very high at the beginning of the blade: 18.93 degrees (ref: figure b9).

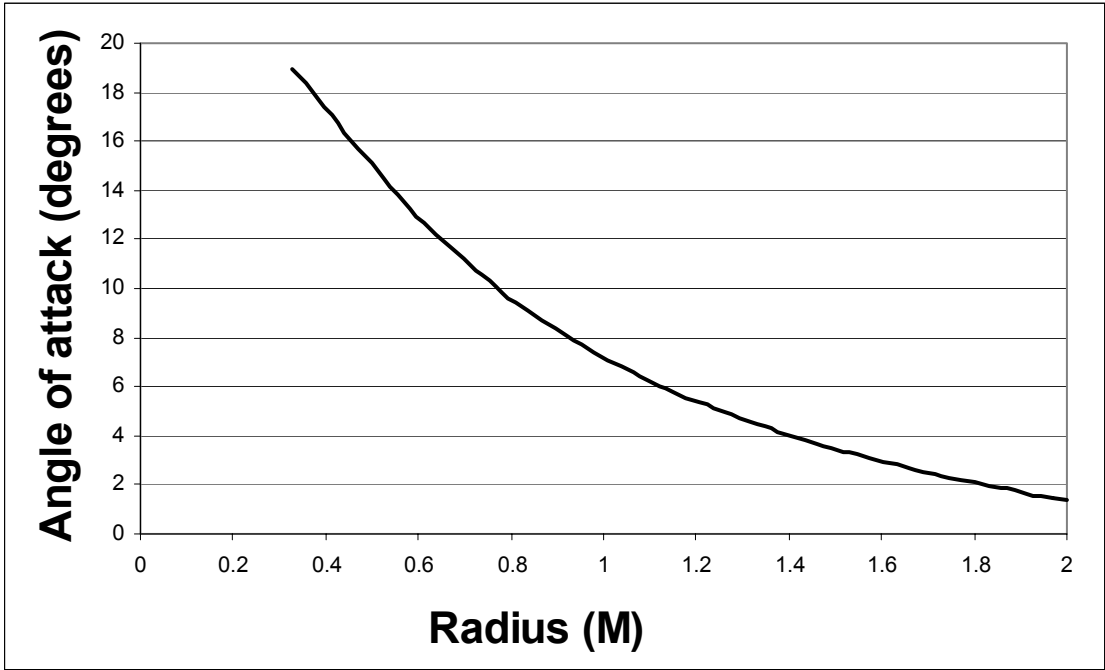


Figure b9: angle of attack on the blade

The data tables providing all the numerical results with the number of iterations made after calculations convergence are available in the appendices. To conclude this chapter, T and Q are given: the total thrust induced by the four blades of the helicopter is calculated: 5734.45 N. In this case, the total Torque is about 1445.45 N.m.

The next step is to use these values of T and Q as input of Fluent Software.

4. Data implementation in FLUENT

The strategy adopted here is to input the data's provided by the previous programme in Fluent. This work represents BEM and CFD coupled calculations.

4.1. Implementation

As in the above method using the momentum theory, the input for the calculations was the blade forces per unit blade length in axial and tangential direction, F_n and F_t , respectively. The Pressures P_n and P_t in axial and tangential direction, respectively, are applied to the actuator disc were derived from the blade forces as follows:

$$P_n = \frac{F_n \cdot N_b}{A} = \frac{F_n \cdot N_b}{\pi \cdot R^2} \quad (\text{eq b.26})$$

$$P_t = \frac{F_t \cdot N_b}{A} = \frac{F_t \cdot N_b}{\pi \cdot R^2} \quad (\text{eq b.27})$$

Where $\left\{ \begin{array}{l} A \text{ is the solid disk area,} \\ N_b \text{ is the number of blades,} \\ r \text{ is the radius.} \end{array} \right.$

The Pressure boundary conditions are applied with the Dynamic Pressure expressed $\frac{1}{2} \rho \cdot V^2$ with User Define Function programmed in C (That does not include the term of static

pressure); the vector directions are input for each element on the disc because of UDF imputation.

4.2. Geometry and Meshes

The disc (with $0.05 R$ thickness) is put in cylindrical domain; the boundaries in the streamwise and spanwise directions are far enough not to perturbate the flow.

In order to limit the interactions with the domain sides, the area is quite big. That implies that node spaces are larger than the previous CFD case. The boundary conditions are exactly identical because that's shown in the first part that it is the best option. Velocity inlets are applied on the disc area and wall condition is functional on the rotor disc side. Symmetry on the study domain sides is the best alternative to reduce boundary effects creating interactions with the flow induced by the helicopter rotor.

The number of mesh nodes is reasonable (200 000 nodes approximately) with non-uniform repartition. The tetrahedral cells are smaller into the first cylinder (Radius: $1.5 R$) and grow into the second cylinder (twice bigger). Finally, the exterior volume gets the bigger spaces between two nodes.

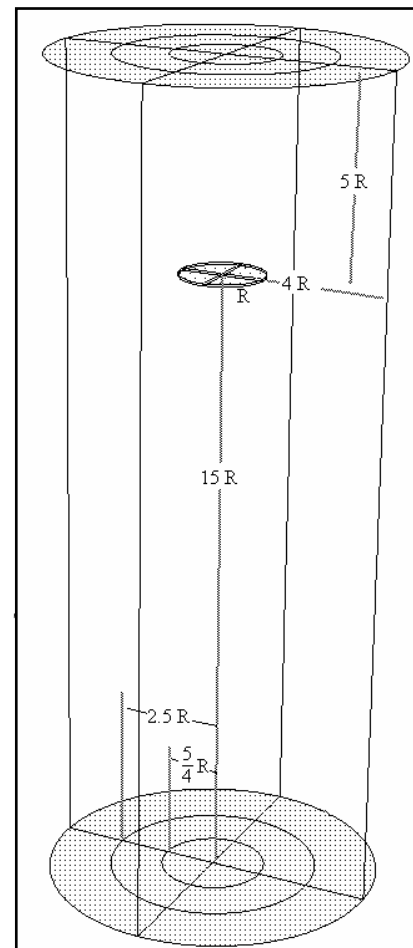


Figure b10: geometry

User Define Function is used with the purpose of imposing the pressure repartitions and its direction vectors on FLUENT. This C program adapted to FLUENT implementation is available in the “appendix 5“.

With the aim of obtaining accuracy data implementation on the rotor, the number of cells on the disc is multiplied with FLUENT until being equal to 1536 quadrilateral faces.

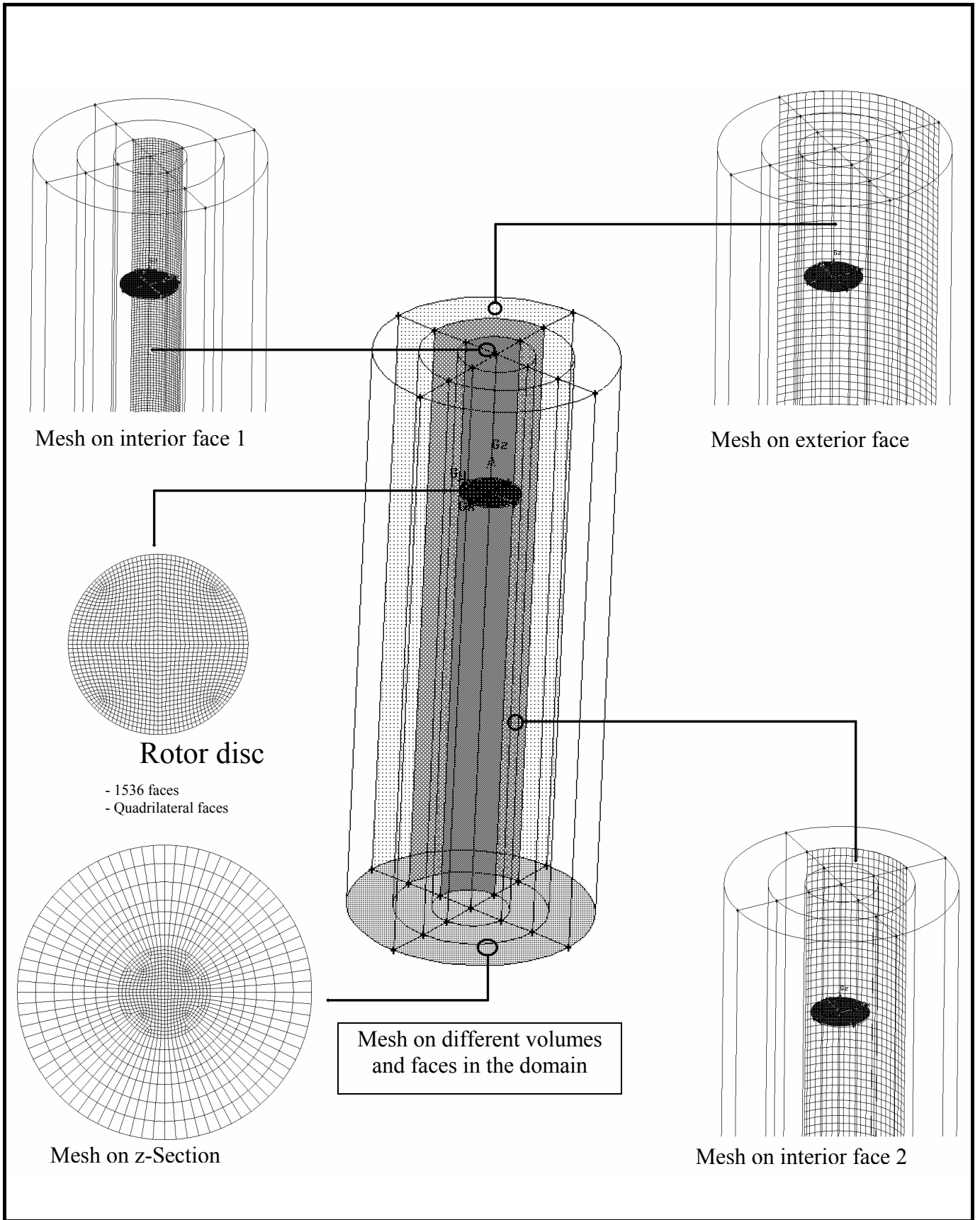


Figure b11: Grid visualisation

4.3. Numerical Procedure

In this case, a turbulent flow is simulated through a real disc. A two-equations RANS model is used, the $k - \varepsilon$ model. All the $k - \varepsilon$ models have similar forms, with transport equations for k and ε . The major differences are the method of calculating turbulent viscosity, the turbulent Prandtl numbers governing the turbulent diffusion of k and ε , the generation and destruction terms in the ε equation. The $k - \varepsilon$ RNG model is applied because it is derived from the instantaneous Navier-Stokes equations, using a mathematical technique called "renormalization group" (RNG) methods. The analytical derivation results in a model with constants different from those in the standard $k - \varepsilon$ model, and additional terms and functions in the transport equations for k and ε . The main interest is that the RNG model in FLUENT provides an option to account for the effects of swirl or rotation by modifying the turbulent viscosity appropriately.

Obviously, the calculation is a steady case. The implicit scheme (Segregated) is privileged to explicit scheme providing difficult convergences. The algorithm, which solves the continuity and momentum equations, is Powerlaw. The Pressure-Velocity coupling solved to get the convergence by the SIMPLE C algorithm. The Standard under relaxation factors are used (Pressure factor: 0.3, Momentum factor: 0.7, Turbuence kinetic energy and turbulent dissipation rate: 0.8).

4.4 Results and discussion

- Validation with the total pressure and thrust

It's important to check the thrust provided by FLUENT in order to validate the implementation by the using of dynamic pressure distribution way described by the previous relations; As the commercial CFD code is not able to calculate this Force alone, velocity magnitude profile is defined and sixth order interpolated in order to calculate the Thrust and the mass flow rate induced by the actuator.

It's assumed that the Thrust is given by the following formula:

$$T = \iint \rho \cdot \vec{V}(r, \theta) \cdot dS \cdot \vec{V}(r, \theta) \quad (\text{eq b.28})$$

A first approximation is to simplify the equation multiplying the mass flow rate with average velocity $|\vec{V}|$:

$$T = \dot{m} \cdot |\vec{V}|$$

So, the mass flow rate definition becomes:

$$\dot{m} = \iint \rho \cdot \vec{V}(r, \theta) \cdot dS$$

$$\dot{m} = \iint \rho \cdot \vec{V}(r, \theta) \cdot r \cdot dr \cdot d\theta$$

It's assumed that $\frac{\partial \vec{V}(r, \theta)}{\partial \theta} = 0$;

$$\dot{m} = 2\pi \cdot \int_{r=R_0}^{r=R_1} \vec{V}(r) \cdot r \cdot dr$$

On the other hand,

$$|\vec{V}| = \frac{1}{R_1 - R_0} \int_{R_0}^{R_1} \vec{V}(r) \cdot dr$$

With R0 and R1 defined in the figure b12:

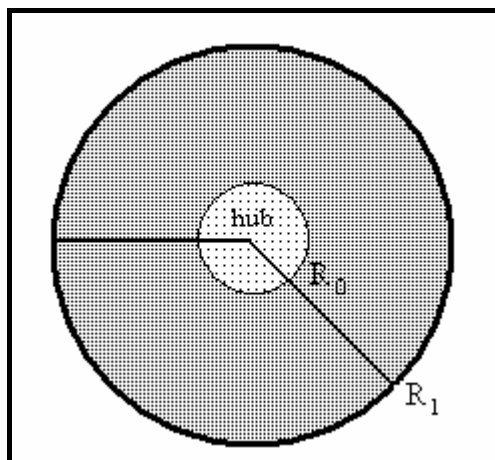


figure b12: disc presentation

With the velocity curve integration, the results are obtained:

$$\left\{ \begin{array}{l} \dot{m} = 271.1439 \text{ kg.s}^{-1} \\ |\vec{V}| = 21.05452 \text{ m.s}^{-1} \end{array} \right.$$

In these conditions, the thrust is found to be equal to:

$$T = 5708.805 \text{ N}$$

To extend the comparison, an estimation of the errors is made It's admitted that T_{Fluent} is the Thrust provided by Fluent, and T_{prog} is the Thrust given by the FORTRAN programme which inputs into the commercial CFD code:

$$\xi = \frac{|T_{\text{prog}} - T_{\text{Fluent}}|}{T_{\text{prog}}}$$

$\xi = 4.472\%$ is the estimated error during the implementation of the data into the CFD code using this methodology.

The thrust provided is only an approximation of the real thrust for the reason that 4.472 % error is declared. To reduce ξ , finer grid should be used, but it would increase the calculation time too much.

To conclude, a supercomputer would have authorized the mesh improving, necessary if better implementation is desired. Furthermore, a CFD code adaptive to helicopter aerodynamics should be tried to check if more exactness is possible with this kind of method.

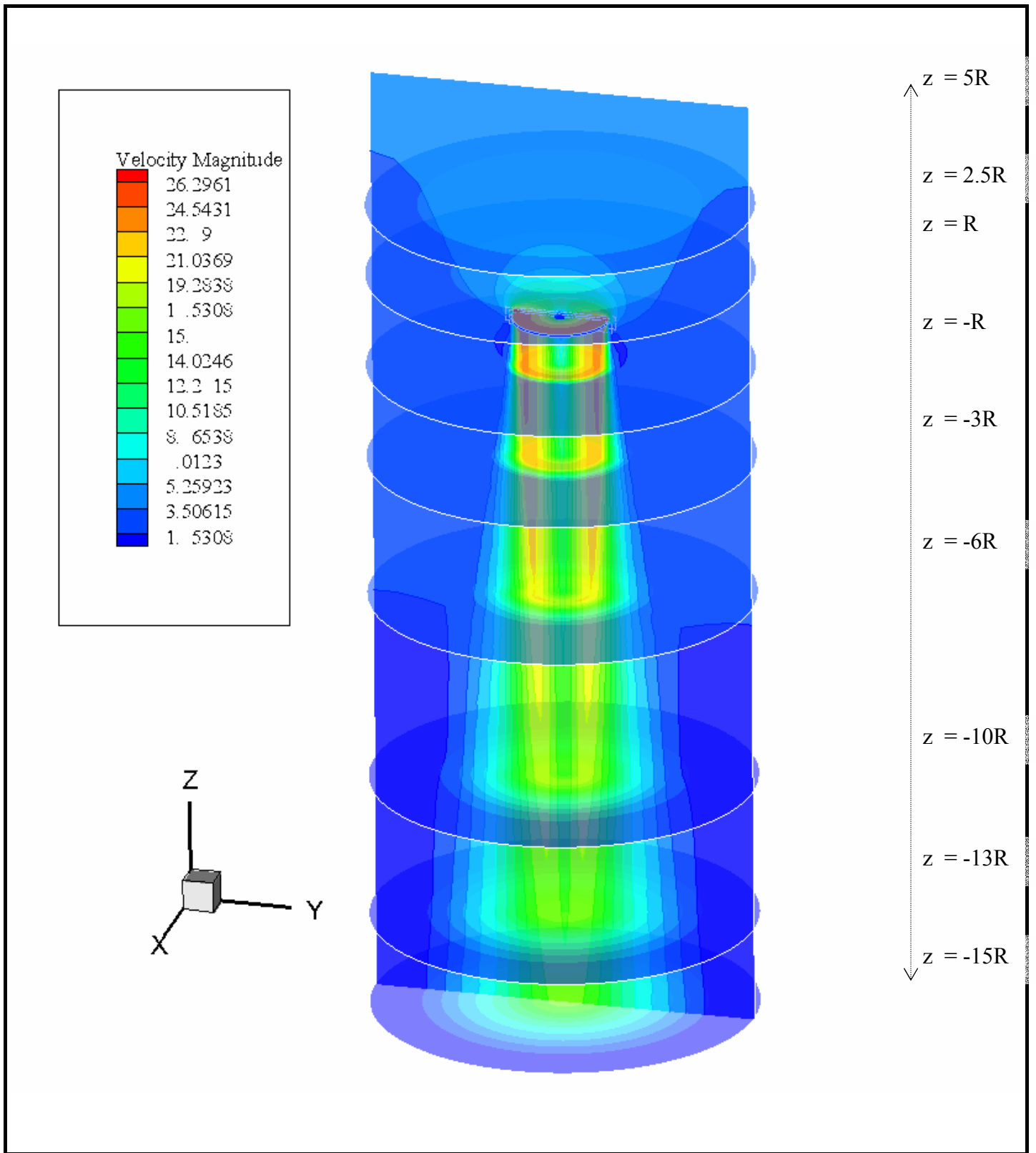


Figure b13: 3-Dimensional Contour Velocity Magnitude at different z coordinates

- Streamlines functions

On figure b14, representing the streamline functions, the expanding core of the vortex is very visible, especially above the 2 diameters distance below the disc. This phenomena is perceptible on figure b14, showing the high velocity expansion below the rotor. The new interest is to discern the rotation induced by the virtual blades. The flow seems to have a radial velocity (because the vortex radius increases along z-axis) whereas the initial conditions impose only the Axial and Tangential velocities.

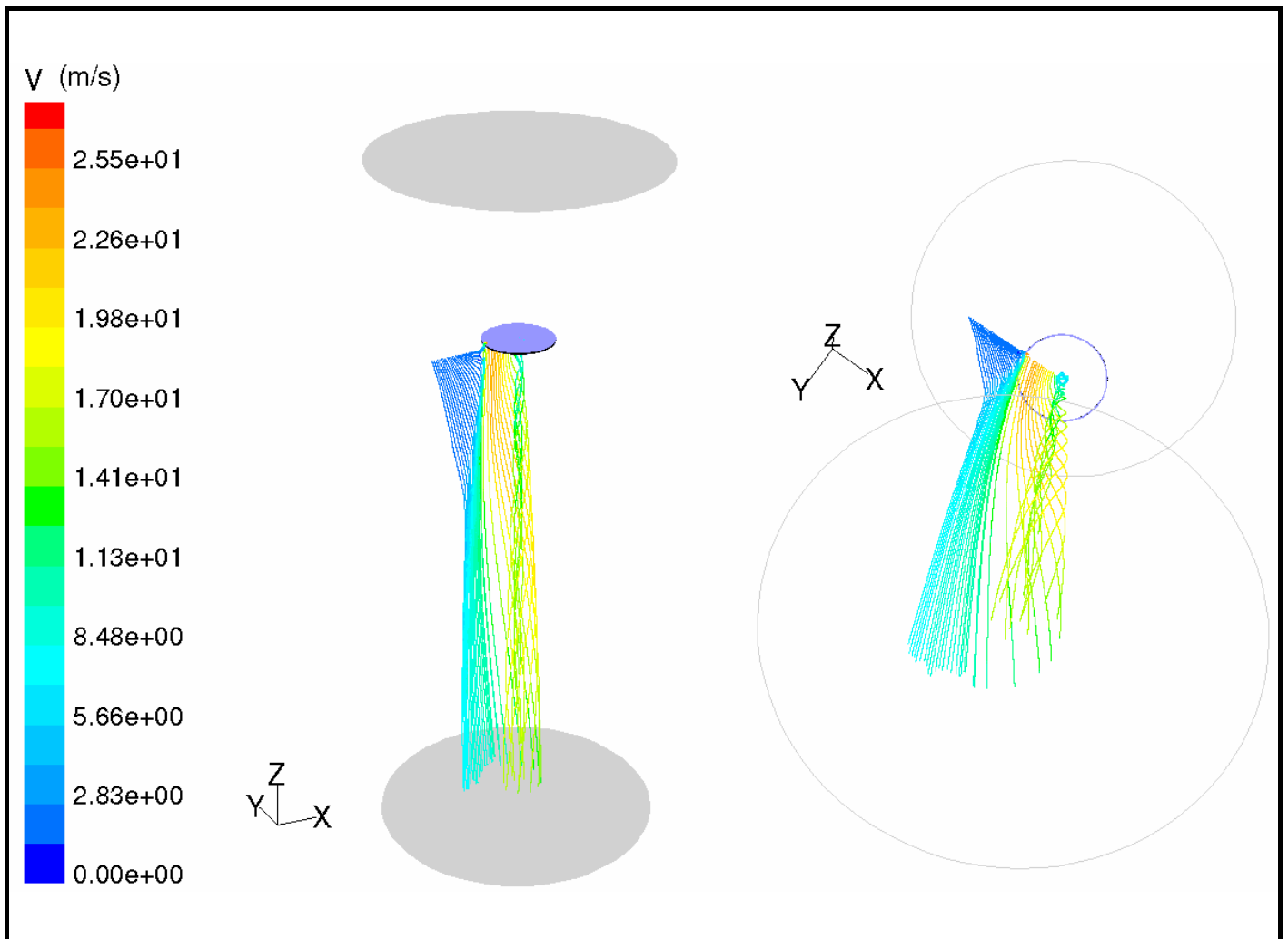


Figure b14: different views of Streamlines Functions

The software is able to give an idea about vorticity measuring the rotation of a fluid element as it moves in the flow field defined by the following relation:

$$\zeta = \nabla \times \vec{V}$$

The high vorticity zones are situated below the disc where the radius is defined by $\{r \in [0;0.5] \cup [1.75;2.5]\}$. The streamline function and vorticity visualisations suggest that the vortex generation is higher if $r > 3R/4$ (ref appendix).

- Dynamic Pressure on the disc

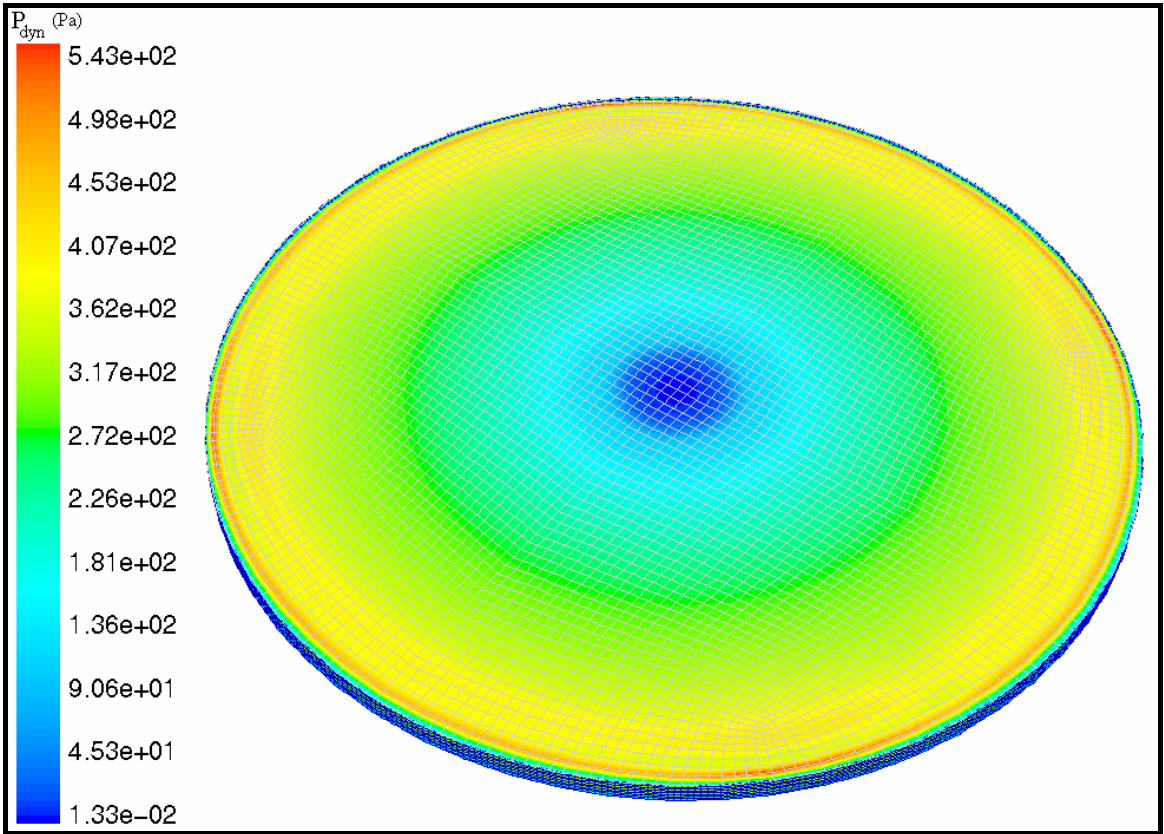


Figure b15: Dynamic Pressure distribution on the disc with the cells visualisation

The first impression is that the pressure values are correct; it is satisfactory to validate using the “User Defined Function”. Despite the fact that the C programme applies no velocity on

the Hub ($r < 0.3\text{m}$), the Dynamic Pressure values are not equal to zero. That includes that the flow induced by the rotor which also induces velocities in the domain ($0 < r < 0.3$).

This issue is not too important if the Pressure values in the Hub (approximately $1.33 \cdot 10^{-2}$) are considered.

- Velocity profiles

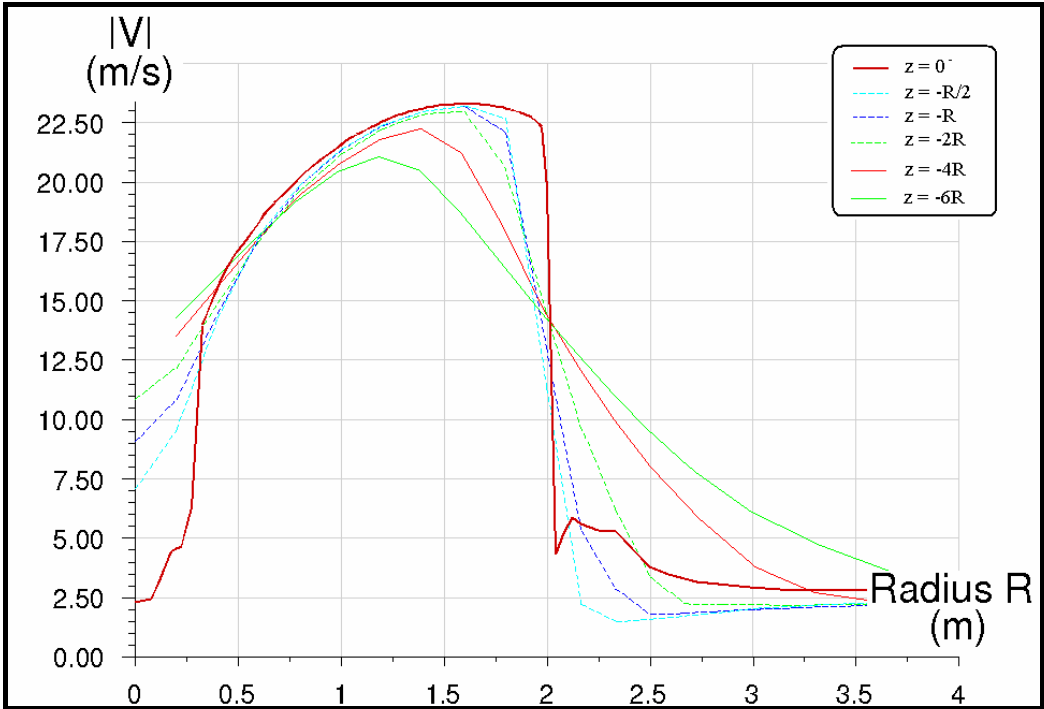


Figure b16: Velocity Magnitude below the rotor

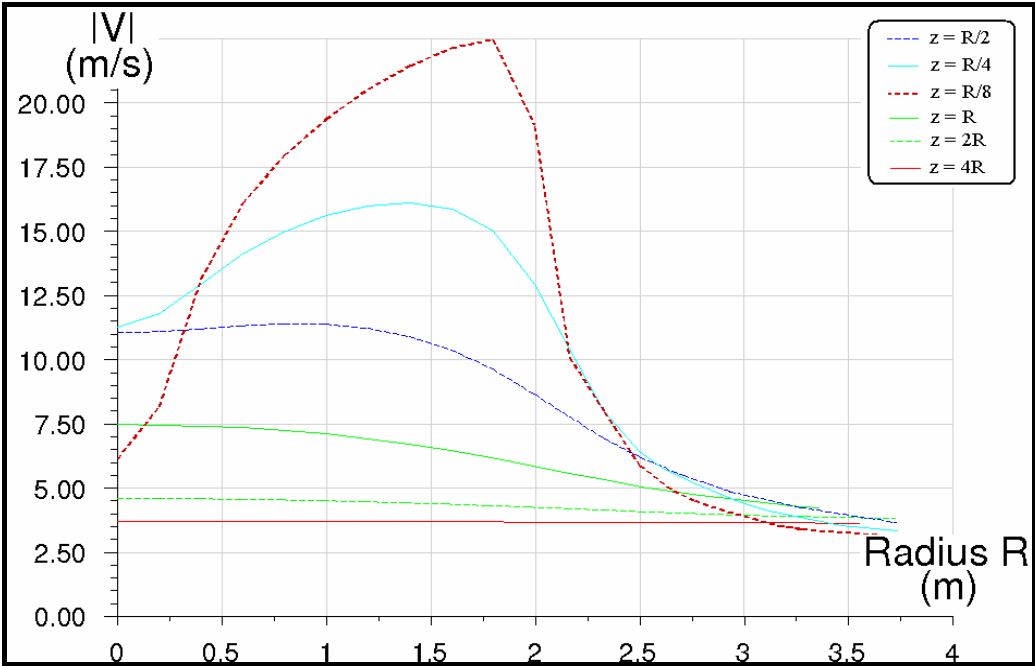


Figure b17: Velocity Magnitude above the rotor

On figure b16, the velocity profiles on lines of control are shown at diverse z coordinates above and below the whole disc. It is fundamental to note the discontinuity on the line $z=0$ which shows the limitations of this grid. In fact, small vortices on the disc sides can appear in the real case but its shapes are generally different. In the domain defined by $\{r \in [0.3; 2]\}$, the velocity repartitions are validated by the software. Using an UDF is the best way to force the non-uniform loading.

The profiles are increasingly flattened when the lines of control are far away. This reveals the vortex core is expanding. The domain size limits seems to be excellent because nothing important happens after 3.5 meters radius even though the domain is a 8 meter radius cylinder to limit interactions with the boudaries.

Figure b17 shows the flow drawn in by the actuator disc. The velocities increase progressively, especially in the sector $r = R$. Even if the flow induced continually gains speed close to the whole disc, a low velocity zone is identified at $z=R/8$ ($z=0.25m$); the simplest explanation is the implementation on the disc of the “drawn in” velocity between $r=0.3 m$ and $r=2m$; checking mass flow rate theory shows that this induces low velocities in the radius $\{r \in [0; 0.3]\}$ simulating the hub of the helicopter rotor system.

- Velocity on the z-axis

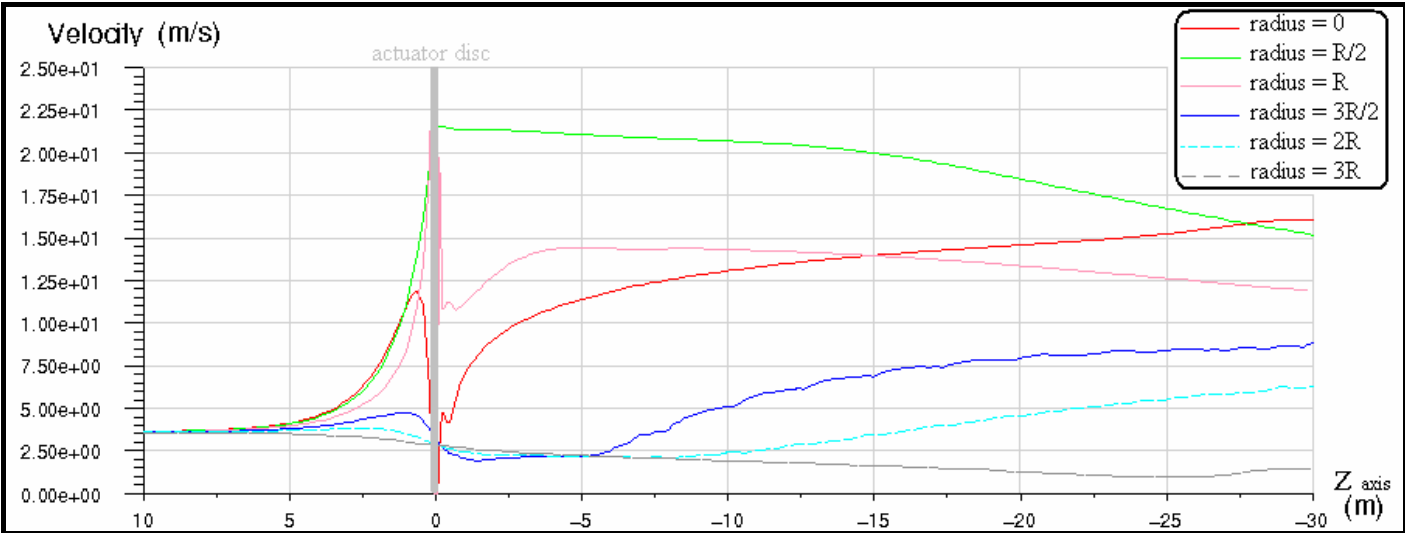


Figure b18: Velocity along Z-axis

Figure b18 shows the velocity magnitude along the Z-axis. The velocity on the “R=0” line increases below the rotor (especially after the coordinates $z = R/2$) and stops its progression at $13.R$ after the whole disc. Numerically, it is not similar to the curves provided by the one-dimensional Momentum theory, but it is assumed that both curves have the same profile. For the two lines taken at $0.5R$ and R , the maximum velocity is on the rotor ($z = 0 \pm 0.1m$). It is interesting to note that the velocity increases progressively after the rotor.

The BEM is a powerful tool for aerodynamic researchers on helicopter rotors. The idea consists of representing the airloads on two-dimensional sections of the blades and integrating their effects in order to find the performance of the rotor as a whole. Whereas simple momentum theory, the blade element approach allows the imputations of blade tip speed, blade loading...

The flow induced by the programme calculation by the way of using CFD code has been reviewed. However, it should be inlightling to compare these results with experimental works or other CFD approaches. But with not enough time, this paper will end without real comparison with other data , which is a huge limitation to this work.

Conclusion

Firstly, a comparison between the data provided by a mathematical study realised by J.T. Conway and a CFD modeling has been made. The methodology and knowledge are employed for the second part.

Secondly, the ideas of combining loading distributions solved with a FORTRAN programme implemented in the commercial CFD code is reviewed. The principles of imputing the blades characteristics in order to obtain lift and drag forces on each blade have been developed. Because of the importance of Reynolds number and Mach number in the force distribution, this method shows its limitations.

It will be possible for other people in the Aerospace and Mechanical Engineering department in UMIST to follow these model studies, in order to ameliorate and compare this results with experimental data.

The goal of the aerodynamic modeling work is to be able to predict the entire flow field around the helicopter rotor and its airframe whatever the flight conditions. Even if this aim has not been achieved, this work is a step forward to that goal.

Appendices

Appendix 1

C program to apply three velocity profiles

Appendix 2

C program to specify “two velocity profiles”
And “jump pressure profile”

Appendix 3

Pictures of dynamic and total pressures, turbulence intensity and turbulent kinetic for the simple rotor

Appendix 4

Pictures of velocity magnitude, axial velocity, radial velocity and tangential velocity on the simple rotor

Appendix 5

FORTRAN Program

Appendix 6

Velocity vectors for the BEM-CFD approach

Appendix 1

C program to apply three velocity profiles

UDF for specifying steady-state velocity profile boundary condition

```
*****
#include "udf.h"
*****

DEFINE_PROFILE(tangentialvelocity, thread , position)
{
    real z[ND_ND];
    real r;
    real U;
    real x;
    real y;
    face_t f;
    begin_f_loop(f, thread)
    {
        F_CENTROID(z,f,thread);
        x=z[0]; y=z[1]; U=20;
        if (sqrt(x*x + y*y) < 1)
        F_PROFILE(f, thread, position) = (-1.5006*sqrt(x*x + y*y)*sqrt(x*x +
        y*y)+1.4972*sqrt(x*x + y*y)+0.0018)*U;
    }
    end_f_loop(f, thread)
}

```

```
DEFINE_PROFILE (radialvelocity, thread , position)

{
    real z[ND_ND];
    real r;
    real U;
    real x;
    real y;
    face_t f;
    begin_f_loop(f, thread)
    {
        F_CENTROID(z,f,thread);
        x=z[0]; y=z[1]; U=20;
        if (sqrt(x*x + y*y) < 0.9)
        F_PROFILE(f, thread, position) = ( 6.4961*sqrt(x*x + y*y)*sqrt(x*x + y*y)*sqrt(x*x +
        y*y)*sqrt(x*x + y*y)*sqrt(x*x + y*y)-12.301*sqrt(x*x + y*y)*sqrt(x*x + y*y)*sqrt(x*x +
        y*y)*sqrt(x*x + y*y)+7.3631*sqrt(x*x + y*y)*sqrt(x*x + y*y)*sqrt(x*x + y*y)-
        2.2472*sqrt(x*x + y*y)*sqrt(x*x + y*y)+0.4579*sqrt(x*x + y*y)-0.0008)*U;
    }
}

```

```

end_f_loop(f, thread)
}

```

```

DEFINE_PROFILE(axialvelocity, thread , position)

```

```

{
  real z[ND_ND];
  real r;
  real U;
  real x;
  real y;
  face_t f;
  begin_f_loop(f, thread)
  {
    F_CENTROID(z,f,thread);
    x=z[0]; y=z[1]; U=20;
    if (sqrt(x*x + y*y) < 0.9)
      F_PROFILE(f, thread, position) = (-1.9033*sqrt(x*x + y*y)*sqrt(x*x + y*y)*sqrt(x*x +
      y*y)*sqrt(x*x + y*y)+1.8453*sqrt(x*x + y*y)*sqrt(x*x + y*y)*sqrt(x*x + y*y)-
      0.3065*sqrt(x*x + y*y)*sqrt(x*x + y*y)+0.2897*sqrt(x*x + y*y)+0.0507)*U;
  }
  end_f_loop(f, thread)
}

```

Appendix 2

C program to specify “two velocity profiles” And “jump pressure profile”

UDF for specifying steady-state velocity and pressure profile boundary condition

```
*****
#include "udf.h"
*****
```

```
DEFINE_PROFILE(tangentialvelocity, thread , position)
{
  real z[ND_ND];
  real r; real U; real x; real y;
  face_t f;
  begin_f_loop(f, thread)
  {
    F_CENTROID(z,f,thread);
    x=z[0]; y=z[1]; U=20;
    if (sqrt(x*x + y*y) < 1)
      F_PROFILE(f, thread, position) = (-1.5006*sqrt(x*x + y*y)*sqrt(x*x +
      y*y)+1.4972*sqrt(x*x + y*y)+0.0018)*U;
  }
  end_f_loop(f, thread)
}
```

```
DEFINE_PROFILE (radialvelocity, thread , position)
{
  real z[ND_ND];
  real r; real U; real x; real y;
  face_t f;
  begin_f_loop(f, thread)
  {
    F_CENTROID(z,f,thread);
    x=z[0]; y=z[1]; U=20;
    if (sqrt(x*x + y*y) < 0.9)
      F_PROFILE(f, thread, position) = ( 6.4961*sqrt(x*x + y*y)*sqrt(x*x + y*y)*sqrt(x*x +
      y*y)*sqrt(x*x + y*y)*sqrt(x*x + y*y)-12.301*sqrt(x*x + y*y)*sqrt(x*x + y*y)*sqrt(x*x +
      y*y)*sqrt(x*x + y*y)+7.3631*sqrt(x*x + y*y)*sqrt(x*x + y*y)*sqrt(x*x + y*y)-
      2.2472*sqrt(x*x + y*y)*sqrt(x*x + y*y)+0.4579*sqrt(x*x + y*y)-0.0008)*U;
  }
  end_f_loop(f, thread)
}
```

```

DEFINE_PROFILE(Pressionaxiale, thread , position)
{
  real z[ND_ND];
  real r; real U; real x; real y;
  face_t f;

  begin_f_loop(f, thread)

  {
    F_CENTROID(z,f,thread);
    x=z[0];
    y=z[1];

    if (sqrt(x*x + y*y) < 1)
    F_PROFILE(f, thread, position) = ( 8521*sqrt(x*x + y*y)*sqrt(x*x + y*y)*sqrt(x*x +
    y*y)*sqrt(x*x + y*y)*sqrt(x*x + y*y)*sqrt(x*x + y*y)-21947*sqrt(x*x + y*y)*sqrt(x*x +
    y*y)*sqrt(x*x + y*y)*sqrt(x*x + y*y)+20741*sqrt(x*x + y*y)*sqrt(x*x +
    y*y)*sqrt(x*x + y*y)*sqrt(x*x + y*y)-9669.3*sqrt(x*x + y*y)*sqrt(x*x + y*y)*sqrt(x*x +
    y*y)+2578.2*sqrt(x*x + y*y)*sqrt(x*x + y*y)-192.33*sqrt(x*x + y*y)-41.65);
  }
  end_f_loop(f, thread)
}

```

Appendix 3

Pictures of dynamic and total pressures, turbulence intensity and turbulent kinetic for the simple rotor

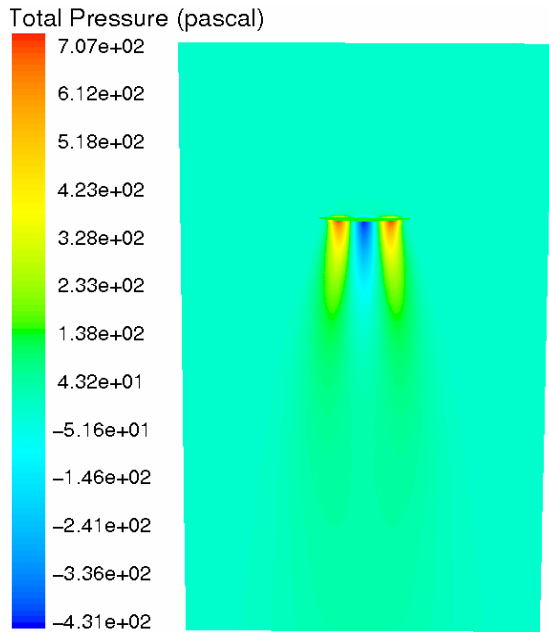


Figure c1: Contour of Total Pressure on a plane

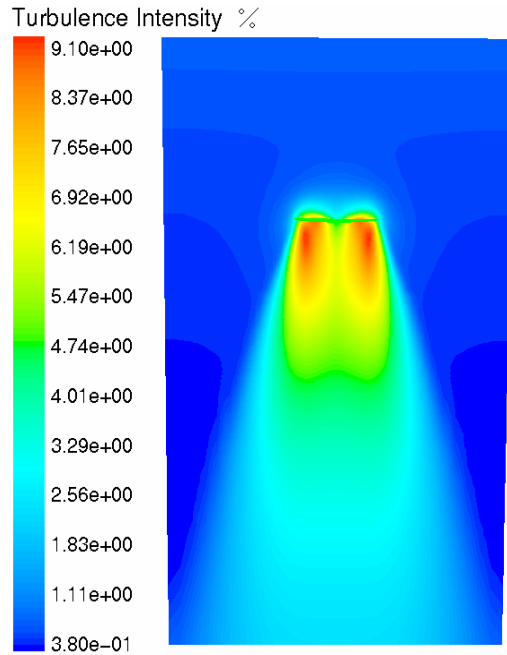


Figure c2: Contour of turbulence intensity on a plane

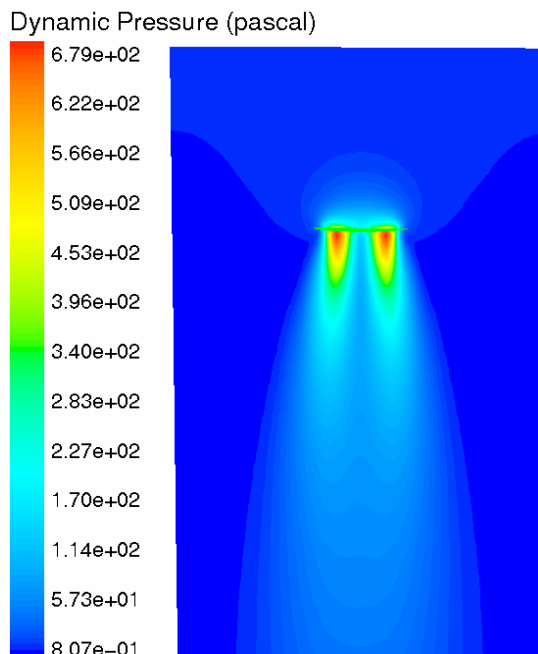


Figure c3: Contour of Dynamic Pressure on a plane

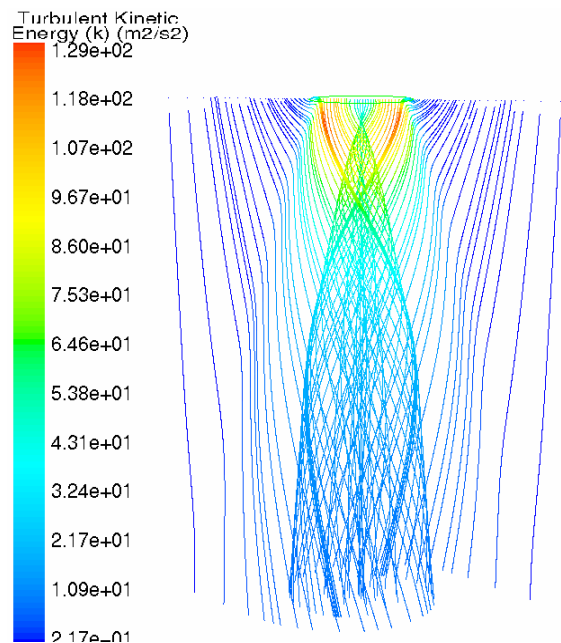


Figure c4: pathlines coloured by turbulent kinetic energy

Appendix 4

Pictures of velocity magnitude, axial velocity, radial velocity and tangential velocity on the simple rotor

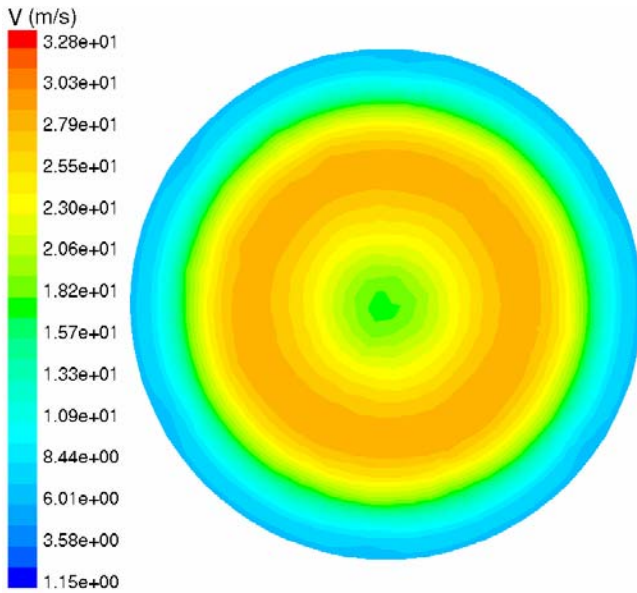


figure c5: Contour of velocity magnitude on the rotor

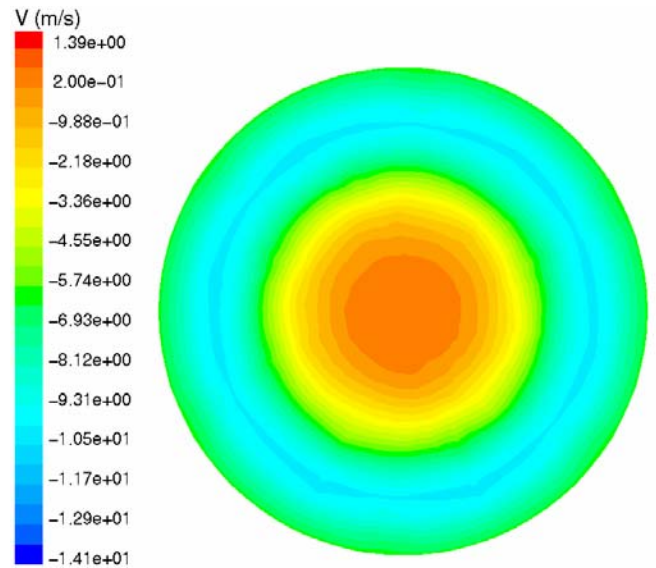


figure c6: Contour of axial velocity on the rotor

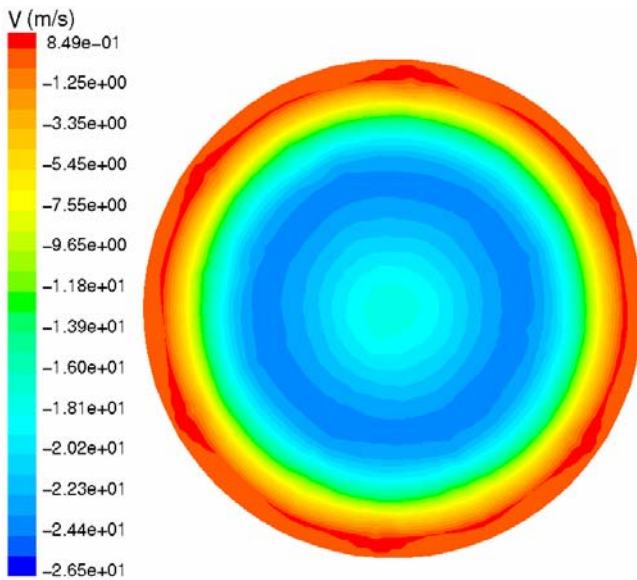


figure c7: Contour of axial velocity on the rotor

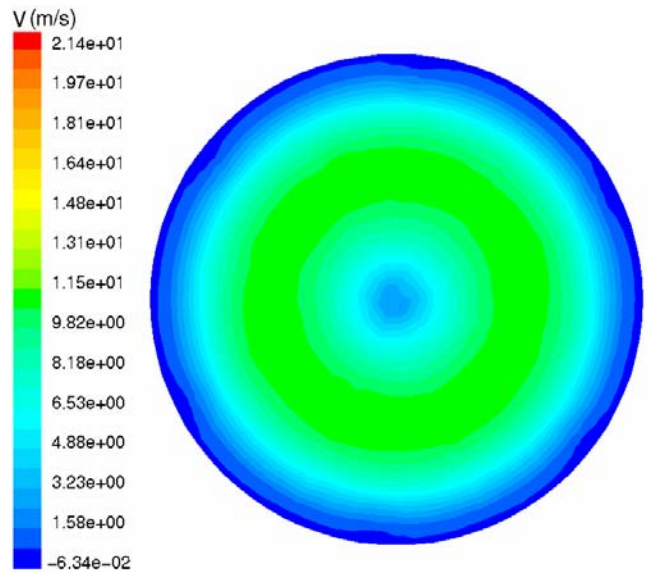


figure c8: Contour of tangential velocity on the rotor

Appendix 5

FORTRAN Program

List of symbols:

Rho	→	ρ density (kg.m ⁻³)
Pi	→	π
Elements	→	Number of elements that divides the blade
r(0)	→	Hub of the rotor system (m)
Uinf	→	Velocity Far away (m.s ⁻¹)
Theta	→	θ angle between the plane of rotation and the Blade (rad)
ww	→	Velocity angle (rad.s ⁻¹)
chord	→	Chord of the NACA airfoil
nn	→	Number of blades
length	→	Length of the blade

program calc

```

integer ii
integer jj
integer iter
integer indice
integer mm
real*8 elements, min
real*8 chord,nn,pi, rho
real*8 a, ap, Uinf, ww
real*8 alpha, alphasad, phi, phi2, theta
real cl, cd, cn, ct
real*8 test1, test2, lenght
real*8 alphatab(1600)
real*8 cltab(1600)
real*8 cdtab(1600)
real*8 diff(1600)
real*8 r(0:200)
real*8 T(0:200), Q(0:200)
real*8 torque(0:200), thrust(0:200)
real*8 sigma(200), phit(200)
real*8 Ft(200), Fn(200)
real*8 pressT(200), pressQ(200), press(200)
real*8 vecteur(200)
real z(100)

rho=1.125
pi=acos(-1.d0)
torque(0)=0.
thrust(0)=0.
elements=80.

```

```

r(0)=0.3
Uinf=35.6
theta=8*pi/180
ww=30*pi
chord=0.16
nn=4.0
lenght=1.7

do jj=1,elements
    r(jj)=(lenght/elements)+r(jj-1)
enddo

```

```

do jj=1,elements

```

```

    a=0.
    ap=0.
    iter=0
    test1=1.
    test2=1.
    cn=0.
    ct=0.
    cd=0.
    cl=0.

```

```

    sigma(jj)=(chord*nn)/(2*pi*r(jj))

```

```

100 do while (abs(a-test1).GT.1.e-5.and.abs(ap-test2).GT.1.e-5)

```

```

    test1=a
    test2=ap

```

```

    phi=(atan(((1-a)*Uinf)/((1+ap)*ww*r(jj))))
    alpha=(phi-theta)
    phit(jj)=alpha*180/pi

```

```

open(20,file='tables1.dat',status='unknown')
write(20,*) alpha
close(unit=20)

```

```

call panel

```

```

open(21,file='tables2.dat',status='unknown')
read(21,*) cd, cl
close(unit=21)

```

```

    iter=iter+1

```

```

cn = cl*cos(phi) + cd*sin(phi)
ct = cl*sin(phi) - cd*cos(phi)
a= 1/(((4*sin(phi)*sin(phi))/(sigma(jj)*cn))+1)
ap= 1/(((4*sin(phi)*cos(phi))/(sigma(jj)*ct))-1)

```

```

write(04,* ) jj, iter, alpha, cl, cd, a, ap

```

```

enddo

```

```

T(jj)=(rho*nn*Uinf*Uinf*(1-a)*(1-a)*chord*cn)/
. (2*sin(phi)*sin(phi))

```

```

Q(jj)=( rho*nn*Uinf*(1-a)*(1+ap)*ww*r(jj)*chord*ct) /
. (2*sin(phi)*cos(phi))

```

```

Fn(jj)=(rho*Uinf*Uinf*(1-a)*(1-a)*chord*cn)/
. (2*sin(phi)*sin(phi))

```

```

Ft(jj)=( rho*Uinf*(1-a)*(1+ap)*ww*r(jj)*chord*ct) /
. (2*sin(phi)*cos(phi))

```

```

thrust(jj)=nn*Fn(jj)*(r(jj)-r(jj-1))+thrust(jj-1)

```

```

torque(jj)=nn*Ft(jj)*(r(jj)-r(jj-1))+torque(jj-1)

```

```

pressT(jj)=nn*Fn(jj)*(r(jj)-r(jj-1))*chord/(pi*r(jj)*r(jj))

```

```

pressQ(jj)=nn*Ft(jj)*(r(jj)-r(jj-1))*chord/(pi*r(jj)*r(jj))

```

```

press(jj)=sqrt(pressT(jj)*pressT(jj)

```

```

+pressQ(jj)*pressQ(jj))

```

```

vecteur(jj)=pressQ(jj)/pressT(jj)

```

```

write(60,* ) r(jj)
write(61,* ) iter
write(62,* ) alpha
write(63,* ) Fn(jj)
write(64,* ) Ft(jj)

```

```

write(11,* ) vecteur(jj)
write(10,* ) pression(jj)
write(09,* ) r(jj)

```

```

enddo

```

```

write(*,* ) '*****'
write(*,* ) 'the thrust is (N)'
write(*,* ) thrust(elements)
write(*,* ) 'the Torque is (N.m) '
write(*,* ) torque(elements)
write(*,* ) '*****'

```

```

        END

c
c  SUBROUTINES
c

subroutine panel

    open(20,file='tables1.dat',status='unknown')
    read(20,*) alpha
    close(unit=20)

    write(*,*) '-----'
    write(*,*) alpha

c
c  smith-hess panel method for single
c  element lifting airfoil in 2-d
c  incompressible flow
c
c  real z(100)
c

    call indata
    call setup

c
c 100 write(6,1000)
c 1000 format(///,' input alpha in degrees')
c   read(5,*)alpha
c   if (alpha.gt.1.5707) go to 200
c
c   cosalf=cos(alpha)
c   sinalf=sin(alpha)
c   call cofish(sinalf,cosalf)
c   call gauss(1)
c   call veldis(sinalf,cosalf)
c   call fandm(sinalf,cosalf)
c   go to 100

200 return
    end

c
c*****
c
c  subroutine setup
c
c  common /bod/ nlower,nupper,nodtot,x(100),y(100),

```

```

2          costhe(100),sinthe(100)
common /num/ pi,pi2inv
c
c pi=3.1415926585
c pi2inv=.5/pi
c
c set coordinates of nodes on body surface
c
c write(6,1000)
c 1000 format(///' body shape'//4x,'x',9x,'y/')
c npoints=nlower
c sign=-1.0
c nstart=0
c do 110 nsurf=1,2
c do 100 n=1,npoints
c fract=float(n-1)/float(npoints)
c z=.5*(1.-cos(pi*fract))
c i=nstart+n
c call body(z,sign,x(i),y(i))
c write(6,1010)x(i),y(i)
c 1010 format(f8.4,f10.4)
c 100 continue
c npoints=nupper
c sign=1.0
c nstart=nlower
c 110 continue
c nodtot=nupper+nlower
c x(nodtot+1)=x(1)
c y(nodtot+1)=y(1)
c
c set slopes of panels
c
c do 200 i=1,nodtot
c dx=x(i+1)-x(i)
c dy=y(i+1)-y(i)
c dist=sqrt(dx*dx+dy*dy)
c sinthe(i)=dy/dist
c costhe(i)=dx/dist
c 200 continue
c
c return
c end
c
c*****
c
c subroutine body(z,sign,x,y)
c
c return coordinates of point on body surface
c
c z = node spacing parameter
c x,y = cartesian coordinates

```

```

c  sign = +1. for upper surface, -1. for lower surface
c
c  common /par/ naca,tau,epsmax,ptmax
c
c  if (sign.lt.0.) z=1.-z
c  call naca45(z,thick,camber,beta)
c  x=z-sign*thick*sin(beta)
c  y=camber+sign*thick*cos(beta)
c
c  return
c  end
c
c*****
c
c  subroutine cofish(sinalf,cosalf)
c
c  set coefficients of linear system
c
c  common /bod/ nlower,nupper,nodtot,x(100),y(100),
c 2          costhe(100),sinthe(100)
c  common /cof/ a(101,111),kutta
c  common /num/ pi,pi2inv
c
c  kutta=nodtot+1
c
c  initialize coefficients
c
c  do 90 j=1,kutta
c 90 a(kutta,j)=0.0
c
c  set vn=0. at midpoint of ith panel
c
c  do 120 i=1,nodtot
c  xmid=.5*(x(i)+x(i+1))
c  ymid=.5*(y(i)+y(i+1))
c  a(i,kutta)=0.0
c
c  find contribution of jth panel
c
c  do 110 j=1,nodtot
c  flog=0.0
c  ftan=pi
c  if (j.eq.i) go to 100
c  dxj=xmid-x(j)
c  dxjp=xmid-x(j+1)
c  dyj=ymid-y(j)
c  dyjp=ymid-y(j+1)
c  flog=.5*log((dxjp*dxjp+dyjp*dyjp)/(dxj*dxj+dyj*dyj))
c  ftan=atan2(dyjp*dxj-dxjp*dyj,dxjp*dxj+dyjp*dyj)
c100 ctimtj=costhe(i)*costhe(j)+sinthe(i)*sinthe(j)
c  stimtj=sinthe(i)*costhe(j)-sinthe(j)*costhe(i)

```

```

a(i,j)=pi2inv*(ftan*ctimtj+flog*stimtj)
b=pi2inv*(flog*ctimtj-ftan*stimtj)
a(i,kutta)=a(i,kutta)+b
if ((i.gt.1).and.(i.lt.nodtot)) go to 110
c
c if ith panel touches trailing edge, add contribution
c to kutta condition
c
a(kutta,j)=a(kutta,j)-b
a(kutta,kutta)=a(kutta,kutta)+a(i,j)
110 continue
c
c fill in known sides
c
a(i,kutta+1)=sinthe(i)*cosalf-costhe(i)*sinalf
120 continue
a(kutta,kutta+1)=-((costhe(1)+costhe(nodtot))*cosalf
2 -(sinthe(1)+sinthe(nodtot))*sinalf
c
return
end
c
c*****
c
subroutine veldis(sinalf,cosalf)
c
c compute and print out pressure distribution
c
common /bod/ nlower,nupper,nodtot,x(100),y(100),
2 costhe(100),sinthe(100)
common /cof/ a(101,111),kutta
common /cpd/ cp(100)
common /num/ pi,pi2inv
dimension q(150)
c
c write(6,1000)
c 1000 format('/// pressure distribution'//4x,'x',8x,'cp'/)
c
c retrieve solution from a-matrix
c
do 50 i=1,nodtot
50 q(i)=a(i,kutta+1)
gamma=a(kutta,kutta+1)
c
c find vt and cp at midpoint of ith panel
c
do 130 i=1,nodtot
xmid=.5*(x(i)+x(i+1))
ymid=.5*(y(i)+y(i+1))
vtang=cosalf*cosche(i)+sinalf*sinthe(i)
c

```

```

c add contributions of jth panel
c
  do 120 j=1,nodtot
    flog=0.0
    ftan=pi
    if (j.eq.i) go to 100
    dxj=xmid-x(j)
    dxjp=xmid-x(j+1)
    dyj=y(y(j))
    dyjp=y(y(j+1))
    flog=.5*a*log((dxjp*dxjp+dyjp*dyjp)/(dxj*dxj+dyj*dyj))
    ftan=atan2(dyjp*dxj-dxjp*dyj,dxjp*dxj+dyjp*dyj)
100 ctimtj=costhe(i)*costhe(j)+sinthe(i)*sinthe(j)
    stimtj=sinthe(i)*costhe(j)-sinthe(j)*costhe(i)
    aa=pi2inv*(ftan*ctimtj+flog*stimtj)
    b=pi2inv*(flog*ctimtj-ftan*stimtj)
    vtang=vtang-b*q(j)+gamma*aa
120 continue
    cp(i)=1.-vtang*vtang
c   write(6,1010)xmid,cp(i)
c 1010 format(f8.4,f10.4)
130 continue
c
  return
  end
c
c*****
c
  subroutine fandm(sinalf,cosalf)
c
c compute and print out cd,cl,cmle
c
  common /bod/ nlower,nupper,nodtot,x(100),y(100),
2          costhe(100),sinthe(100)
  common /cpd/ cp(100)
c
  cfx=0.0
  cfy=0.0
  cm=0.0
c
  do 100 i=1,nodtot
    xmid=.5*(x(i)+x(i+1))
    ymid=.5*(y(i)+y(i+1))
    dx=x(i+1)-x(i)
    dy=y(i+1)-y(i)
    cfx=cfx+cp(i)*dy
    cfy=cfy-cp(i)*dx
    cm=cm+cp(i)*(dx*xmid+dy*ymid)
100 continue
  cd=cfx*cosalf+cfy*sinalf
  cl=cfy*cosalf-cfx*sinalf

```

```

open(21,file='tables2.dat',status='unknown')
write(21,*) cd, cl
close(unit=21)

c write(6,1000)cd,cl,cm
c 1000 format(////' cd =,f8.5,' cl =,f8.5,' cm =,f8.5)
c
c return
c end
c
c*****
c
c subroutine gauss(nrhs)
c
c solution of linear algebraic system by
c gaussian elimination with partial pivoting
c
c [a] = coefficient matrix
c neqns = number of equations
c nrhs = number of right-hand sides
c
c right-hand sides and solutions stored in
c columns neqns+1 thru neqns+nrhs of a
c
c common /cof/ a(101,111),neqns
c
c np=neqns+1
c ntot=neqns+nrhs
c
c gauss reduction
c
c do 150 i=2,neqns
c
c search for largest entry in (i-1)th column
c on or below main diagonal
c
c im=i-1
c imax=im
c amax=abs(a(im,im))
c do 110 j=i,neqns
c if (amax.ge.abs(a(j,im))) go to 110
c imax=j
c amax=abs(a(j,im))
110 continue
c
c switch (i-1)th and imaxth equations
c
c if (imax.ne.im) go to 140
c do 130 j=im,ntot

```

```

    temp=a(im,j)
    a(im,j)=a(imax,j)
    a(imax,j)=temp
130 continue
c
c eliminate (i-1)th unknown from
c ith thru neqnsth equations
c
140 do 150 j=i,neqns
    r=a(j,im)/a(im,im)
    do 150 k=i,ntot
150 a(j,k)=a(j,k)-r*a(im,k)
c
c back substitution
c
    do 220 k=np,ntot
    a(neqns,k)=a(neqns,k)/a(neqns,neqns)
    do 210 l=2,neqns
    i=neqns+1-l
    ip=i+1
    do 200 j=ip,neqns
200 a(i,k)=a(i,k)-a(i,j)*a(j,k)
210 a(i,k)=a(i,k)/a(i,i)
220 continue
c
    return
    end
c
c*****
c
    subroutine indata
c
c set parameters of body shape, flow
c situation, and node distribution
c
c user must input:
c nlower = number of nodes on lower surface
c nupper = number of nodes on upper surface
c plus data on body
c
    common /bod/ nlower,nupper,nodtot,x(100),y(100),
2          costhe(100),sinthe(100)
    common /par/ naca,tau,epsmax,ptmax
c
    nlower=30
    nupper=30

    naca=20012
c
    iep= naca/1000
    iptmax=naca/100-10*ieps

```

```

itau=naca-1000*ieps-100*iptmax
epsmax=ieps*0.01
ptmax=iptmax*0.1
tau=itau*0.01
if (ieps.lt.10) return
ptmax=0.2025
epsmax=2.6595*ptmax**3
c
  return
  end
c
c*****
c
  subroutine naca45(z,thick,camber,beta)
c
  common /par/ naca,tau,epsmax,ptmax
c
c evaluate thickness and camber
c for naca 4- or 5-digit airfoil
c
  thick=0.0
  if (z.lt.1.e-10) go to 100
  thick=5.*tau*(.2969*sqrt(z)-z*(.126+z*(.3537
  2      -z*(.2843-z*.1015))))
100 if (epsmax.eq.0.) go to 130
  if (naca.gt.9999) go to 140
  if (z.gt.ptmax) go to 110
  camber=epsmax/ptmax/ptmax*(2.*ptmax-z)*z
  dcamdx=2.*epsmax/ptmax/ptmax*(ptmax-z)
  go to 120
110 camber=epsmax/(1.-ptmax)**2*(1.+z-2.*ptmax)*(1.-z)
  dcamdx=2.*epsmax/(1.-ptmax)**2*(ptmax-z)
120 beta=atan(dcamdx)
c
  return
c
130 camber=0.0
  beta=0.0
c
  return
c
140 if (z.gt.ptmax) go to 150
  w=z/ptmax
  camber=epsmax*w*((w-3.)*w+3.-ptmax)
  dcamdx=epsmax*3.*w*(1.-w)/ptmax
  go to 120
150 camber=epsmax*(1.-z)
  dcamdx=-epsmax
  go to 120
c
  end

```

Appendix 6

Velocity vectors for the BEM-CFD approach

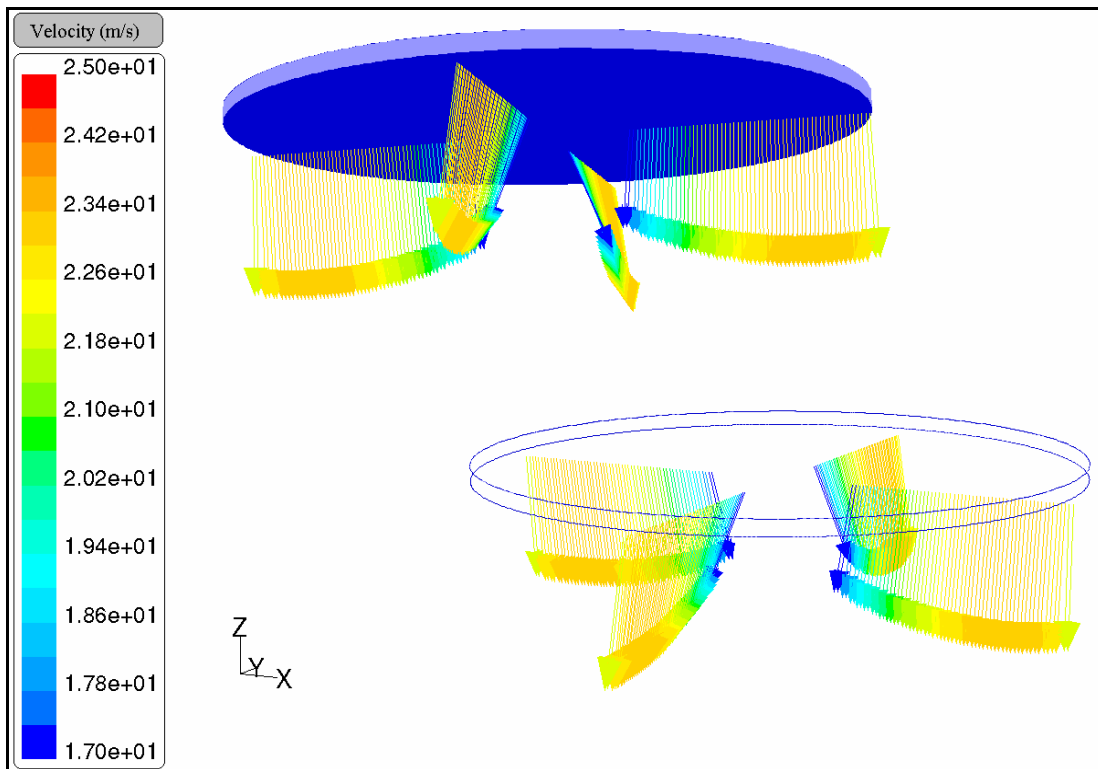


Figure c9: Velocity vectors on the disc coloured by velocity magnitude

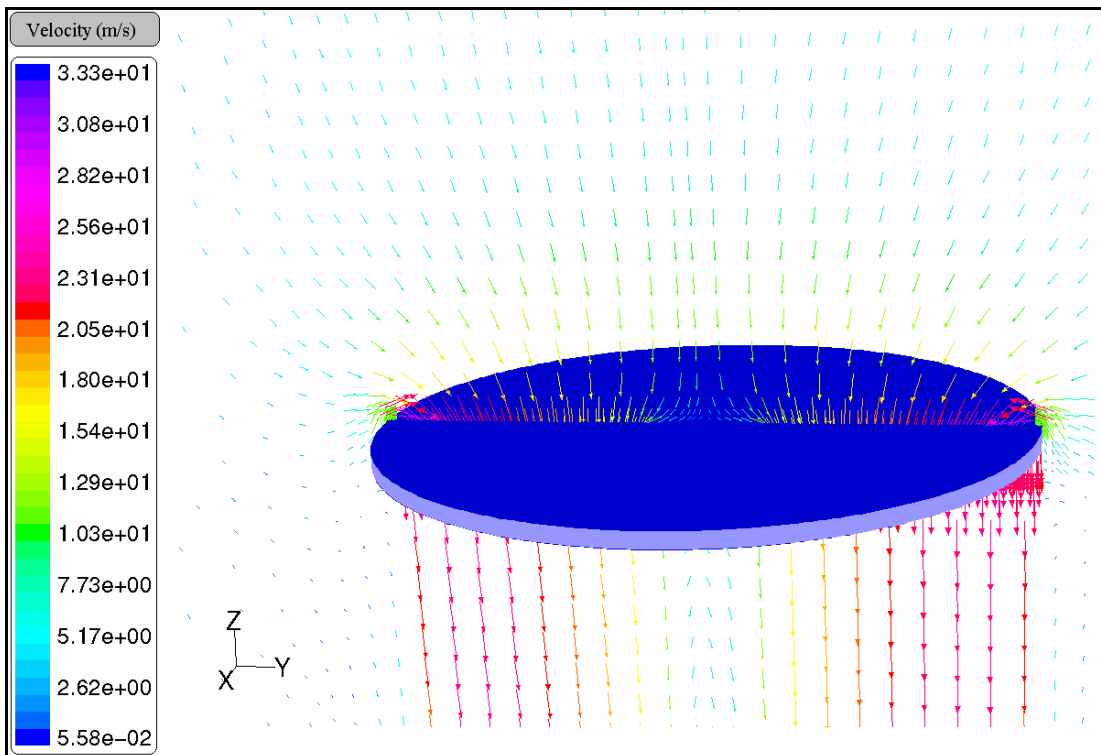


Figure c10: Velocity vectors on a plane coloured by velocity magnitude

References

Rotary-wing aerodynamics

Vol 1: *basic theories of rotor aerodynamics*

Vol 2 : *performance prediction of helicopter*

W.Z.Stepniewsky and C.N.Keys

Dover publications, Inc., New York.

Exact actuator disk solutions for non-uniform heavy loading and slipstream contraction

J.T.Conway

(J. Fluid Mech. (1998) Vol. 365, pp 235-267)

Principles of Helicopter Aerodynamics

J. Gordon Leishman

Cambridge Aerospace Series

Simulating Dynamical Behaviour of Wind Power Structures

Anders Ahlström

Licentiate Thesis, Stockholm, 2002

Royal Institute of Technology - Department of Mechanics

AERFORCE: Subroutine Package for unsteady Blade-Element/Momentum Calculations.

Anders Björck

Flygtekniska Forsöksanstalten

The Aeronautical Research Institute of Sweden

Actuator disc modelling for helicopter rotor

Frederic Le Chuiton

DLR – Institute of Aerodynamics and Flow technology

Braunschweig, Germany

Airfoil Characteristics for Wind Turbines

Christian Bak, Peter Fuglsang, Niels N. Sørensen, Helge Aagaard Madsen

Risø National Laboratory (March 1999)

Wen Zhong Shen, Jens Nørkær Sørensen

Technical University of Denmark

AIAA publications (V22 Osprey)

American Institute of Aeronautic and Astronautic